„POLITEHNICA" UNIVERSITY of BUCHAREST

FACULTY OF MECHANICAL ENGINEERING AND MECHATRONICS

MACHINE ELEMENTS AND TRIBOLOGY DEPARTMENT

Senate Decision No. / 30.06.2017

DOCTORAL THESIS
-ABSTRACT-

CONTRIBUŢII LA REDUCEREA EXCITAŢIILOR PARAMETRICE LA ANGRENAJELE CILINDRICE CU DINŢI ÎNCLINAŢI
CONTRIBUTIONS TO PARAMETRIC EXCITATION REDUCTION AT HELICAL GEARS

Author: Ing. **Ionel Sorin GABROVEANU**

DOCTORAL COMISSION

President	Prof.dr.ing. Octavian DONȚU	From	University „Politehnica" București
Doctoral tutor	Prof.dr.ing. Andrei TUDOR	From	University „Politehnica" București
Referent	Prof.dr.ing. Vasile BOLOȘ	From	University „Petru Maior" Târgu Mureș
Referent	Dr.ing. Valentin SILIVESTRU	From	INCDT-COMOTI București
Referent	Conf.dr.ing Victor MARIAN	From	University „Politehnica" București

Bucharest, 2017

Content

Notations

a	Distance between axles
b	Gear width
d_a	Tip diameter
d_b	Base diameter
d_g	Profile root correction diameter
d_L	Active profile start diameter
d_m	Median diameter
f_z	Meshing frequency
i	Current contact line index
k_γ	Meshing stiffness
l_k	k Contact line length
m_n	Normal module
p_{bt}	Front base step
$r_{b1,2}$	Base radius
x	Specific profile shift
y	Coordinate
z	Coordinate. Teeth number
α_{wt}	Frontal meshing pressure angle
A, B, C, D, E	Characteristic points on meshing line
F_n	Normal force
L_h , L_σ	Accoustic transmission functions
$L_F(f)$	Vibrational power spectrum
$L_W(f)$	Radiant power spectrum
N	Natural number class
T	Torque
β	Helix angle, reference
δ	Tooth deflexion
ε_α	Gradul de acoperire frontal
ε_β	Gradul de acoperire axial (suplimentar)Overlap
$\varepsilon_{\gamma r}$	Gradul de acoperire total real
φ	Relative rotation angle between gears
$\Delta_{\alpha a}$	Head correction depth, normal
1,2	Pinion, gear index

1. GENERAL CONSIDERATIONS

1.1. Short view on research area

To see motivations of the research in ideea of use of active actions in vibroacoustic of the gears, strat point is the analysis of the actual and future issues.

Today's and future basic directions in machinery domain are:

1. Increasing of the fiability;
2. Weight and volume reduction for technical systems.

Almost all mechanical systems contain gear transmission which in most cases determin their volume, the reduction of gear volume is the first way, as importance. Mainly, the ways to obtain this are (Sauer, 1970 b):

1. Load capacity improvement;
2. Use of modern computing methods.

Most important way is the improvement of the load capacity. In the following rows, are presented the ways to improve the load capacity for gears:

1. Increse of internal dynamic quality of the meshing gears, in order to reduce the dynamic internal loads;
2. Constructive and technological ways, as:
   a) Use of helical gears, having incresed load capacity compared to spur gears;
   b) Gear geometry corrections, assuring increased load capacity;
   c) Extrapolar gears;
   d) Use of new lubricants;

This presentation underline the importance of the measures aimed to improve the internal dynamic behaviour of the meshing gears. This measures remains actual for the spur and helical gears, where internal excitations are high.

Using the active measures to reduce parametric vibrations are assured the directions of the machinery development described previously.

1.2. Scope and work objectives

Actual situation analysis in this field will be performed in the present work and will confirm the scope and the objectives already mentioned below.

Scope. Present work study the posibility to apply active measures to improve the vibroacoustic behaviour of the helical evolventic gears, using the parametric excitation reduction.

Objectives necessary to be attained to reach the scope are presented below:

1. Analysis of the actual stage for theoretical and experimental research;
2. Theoretical research regarding the influence of the overlap factor equal to unity on:
   a) Meshing stiffness;
3. Experimental research to confirm the theoretical results obtained;
4. Final conclusions.

1.3. Scientific and applicative work importance

Combined research, theoretic and experimental has as finality the production of the helical meshing gears with improved vibroacoustic behaviour, having the previous underlined advantages: increased fiability, increased operating life, reduced volume.

Chapters from actual work are written using the expertize acquired in contracts where COMOTI and the author were involved, STARTGENSYS and ELTESTSYS, for example, financed by EU, having as objective to realize high performance test rigs, including high speed geared transmissions. Theoretical solutions discussed in this work were applied on COMOTI products sold to national and international customers, most important case being the one of the three stage intercooled compressor sold to LINDE – GAS International.

One important point in aircraft gears study in Europe, more precisely the relaunch of the research was the start of the ESPOSA contract, signed in October, 2011. Under this contract, the author of the present paper was in charge with

- Experimental study of bending strength (STBF);
- Pitting, scuffing and scoring tests.

2. ACTUAL LEVEL OF RESEARCH

2.1. Introduction

Day's status realized in following chapter has as objectiv to justify the actuality of the thesis subject. In this idea are briefly presented results contained in reference works in this domain. The directions are the following:

1. Excitation types and their comparative effect on helical gears, showing the overwhelming role of the parametric excitation on vibroaciustic behaviour of the gears;
2. Aspects on theoretic and experimental parameters defining the parametric excitation (gears deformation, excitation defining methods).

2.2. Actual level of theoretical research

2.2.1. Excitement sources, comparative effects on vibroacoustic behaviour of gears

Picture 2.1 classifiess the excitation souces for gears. On first place, the variable mesh stiffness.

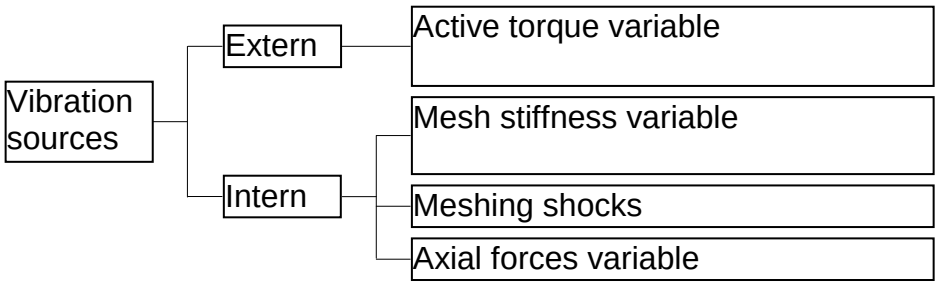

Figura 2.1. Excitation sources in gears(by Dobre, Mirica, Gabroveanu, 2008)

Almost all researchers consider as important as important internal excitation sources, interfering with the exact cinematic of the meshing:

1. Total gears stiffness, time dependent, for spur and helical gears; this variation determine the meshing gear parametric excitation;
2. Meshing shocks due to:

   a) Geometry errors due to manufacturing and assembly;

   b) Gears deformation, determining entry and output in exterior of theoretic area- premature entry and delayed output in meshing area.

   As will be later shown, the literature underlines that most important excitations remains the parametric excitation and the meshing shocks, mainly because today the gears are realized with high precision and these excitations became more important than geometric errors.

These main excitations could be reduced using active methods, acting in ideea to reduce excitation on source and not to passive atenuation of the effects.

2.2.2. Actual stage of the theoretical research

2.2.2.1. introduction

Below is presented the daily stage in the area linked to the scope and objectives of this work:

- Gear deformation imposed by internal excitations (time variation of the gear stiffness);
- Meshing gear excitation;
- Results obtained by researchers in this study area.

2.2.2.2. Actual stage in cylindrical gears deformation

Due to the huge importance of the gears deformation problem in defining the problem of the deformation of the gears under load, excitations too, these were studied both theoretical and practical even many years ago.

Research on gear deformation intensifies over time, in parallel with technical progress in the domain of the measuring devices. As first works, are to be underlined those of **Kistian (1948), Korovcinski (1949), Andojski (1951)**, **Weber and Banaschek (1953)**, **Kistian and Frenkel (1956), Rettig (1957)**, **Schlaf (1962)**.

As elastic deformation models for the tooth representatives are the following:

1. **Beamed beam model,** based on classical definition. Model was reused later by **Andojski şi Efimovici (1959),** but experiments were not convincing.
2. The model based on plane stress of defomation **(Weber, Banaschek, 1953)** takes into account (spur tooth) on the dimensional report of the part. Ipothesis is full justified, as mentioned earlier, tooth length being much greater than the others dimensions. As follows, instead plane state of stress $\sigma_z = 0$ appears plane state of deformation $\varepsilon_z = 0$. Picture 2.2 presents loading scheme for this computing model and the method to determine the tooth width at root $\bar{s}_f$;
3. The third model is infinite wedge model, but being based on simplifying assumptions produces non valid results.
4. **Plate elastic beamed model**

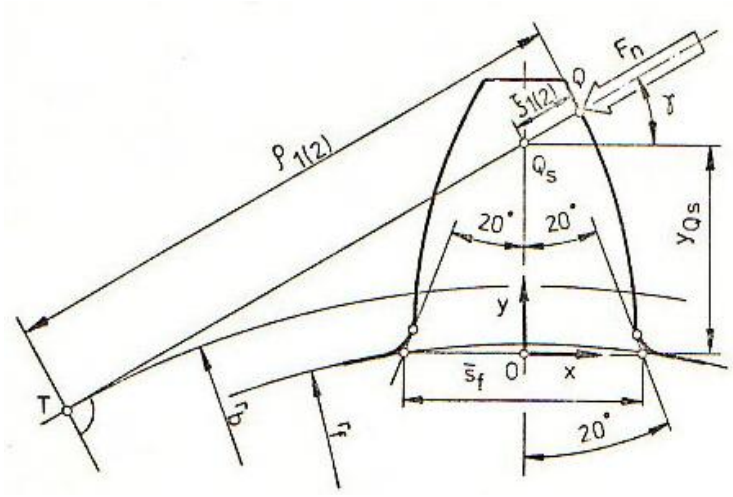

Figura 2.2. Schema de calcul a componentelor deformaţiei danturii (Weber, Banaschek, 1953)

This model is practically justified, the results being congruent with experiement. Supplementary, could be used for spur gear and helical gear, with good results **(Ziegler, 1971).**

The evaluations are centered in principal on spur gear; some aspects linked to the ovarlap factor are made in subchapter 2.4.3.2.

For helical gears, different variations of the mesh stiffness are presented after **Ziegler (1971)** in pictures 2.3...2.4. Could be observed that these pictures includes cases for variations for total overlap real equal to 2 (picture 2.3) and 3 (picture 2.4). Only for $\varepsilon_{\gamma r} = 3$ is observed an severe attenuation of the variation of neshing stiffness, but unsustained fenomenologically by Ziegler.

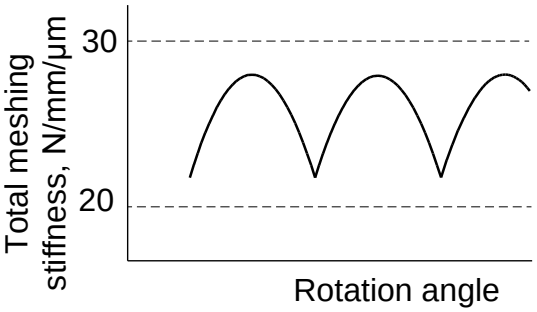

Picture 2.3. Mesh stiffness variation for $\varepsilon_{\gamma r} = 2$ (Ziegler, 1971)

a=125 mm, m=2,5 mm, b=70 mm, $z_1=z_2=46$, $x_1=x_2=0$, $\beta=23^o\ 4'\ 26''$, $F_n/b=240$ N/mm.

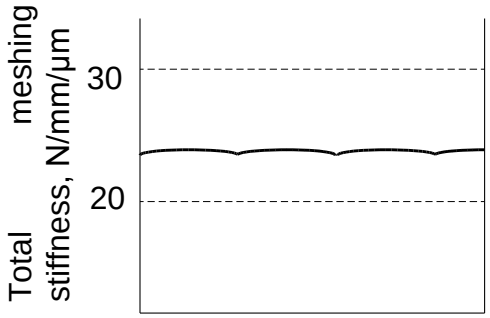

Picture 2.4. Mesh stiffness variation for $\varepsilon_{\gamma r} = 3$ (Ziegler, 1971)

a=125 mm, m=2,5 mm, b=70 mm, $z_1=z_2=46$, $x_1=x_2=0$, $\beta=23^o\ 4'\ 26''$, $F_n/b=240$ N/mm.

Variable force acting on the tooth has considerable influence on the vibratory behaviour and on the meshing noise.

A particular method to define the stiffness was formulated by **Dobre (1987),** which considers premature meshing and delayed mesh exit outside the meshing line, using the so-called functional backlashes. As a result, he demonstrated that the variation of meshing stiffness are not sudden (picture 2.5), confirming experiments of **Rettig (1957).** Picture 2.6 upon **Dobre (2006),** prove that the meshing shocks appear, the profile correction being necessary. The gears were considered as being without geometric errors, driving gear being 1. Even in such a situation, premature entry in meshing in A and delayed meshing exit in D are a notable excitation source.

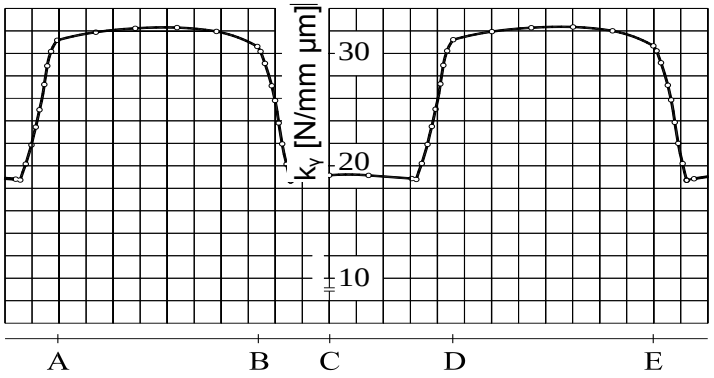

Picture 2.5. Static stepped variation of the meshing stiffness along the meshing line, spur gears (upon Dobre, Mirica, Gabroveanu, 2008)

$a = 125\ mm;\ m = 4\ mm;\ \beta = 0^o;\ z_1 = 23;\ z_2 = 37;\ x_1 = 0{,}69;$
$x_2 = 0{,}733;\ b = 46mm;\ T_1 = 784{,}4\ Nm.$

Capabilities and limits of such measures for such measures were discussed by **Storm (1980).** The tonal character of the emitted noise remains unchanged, due to the wideband action of such measures. As first oder measure, of central importance is to reduce the vibration level of the meshing gears.

Chong, Myong și Kim (2001) considered the transmission error (produced by manufacturing errors) as a vibration source. Starting from this point, their work studyied simultaneous computation of the profile modification minimizing the excitations on helical gears. A parameter named aspect report is used, being the raport between gear width and division diameter (picture 2.7).

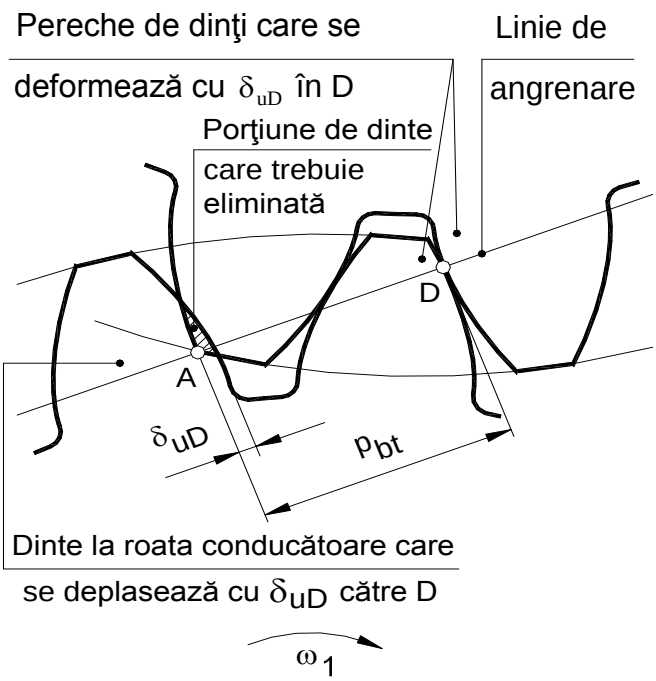

Figura 2.6. Explicaţia apariţiei şocurilor de angrenare

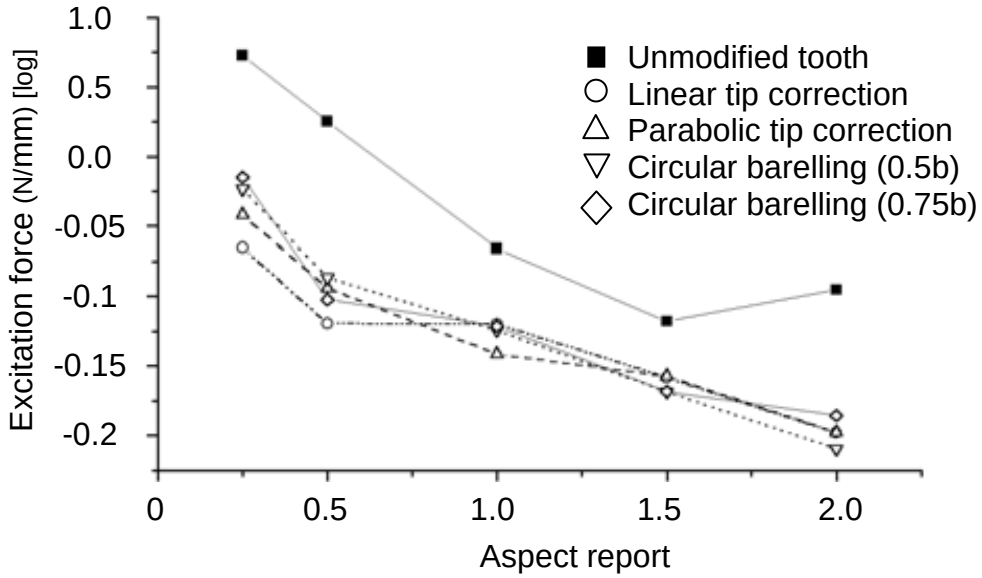

Picture 2.7. Excitation force, helical gears, function of aspect report (upon Chong, Myong and Kim, 2001)

Ziegler (1971) has as job meshing stiffness and the load distribution in the meshing gears. He studied the effect of the total overlap parameter on the meshing gear stiffness, and on the vibratory overload of the gears. The situation is described in picture 2.8.

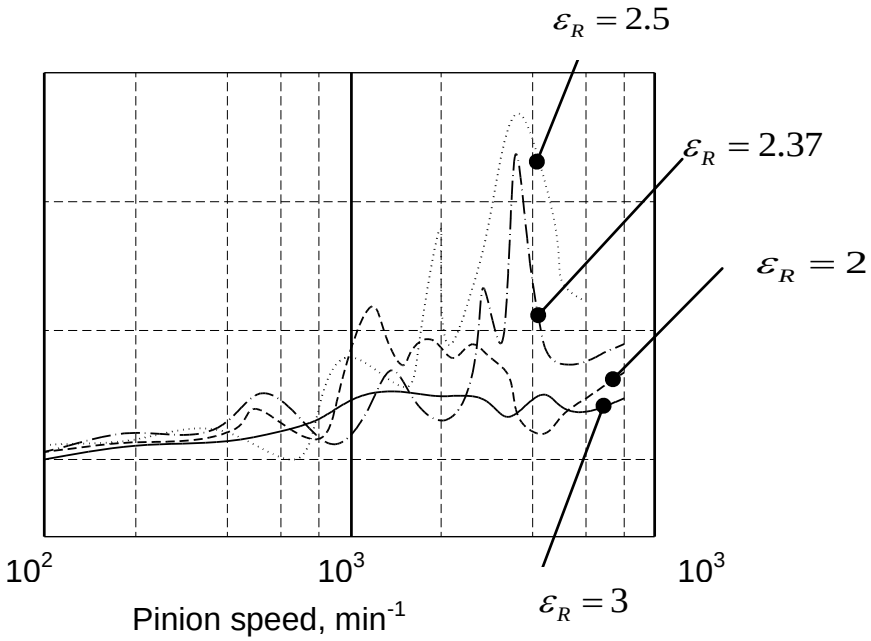

Picture 2.8. Dinamic overload factor (upon Ziegler, 1971)

2.3. Actual stage for experimental research

2.3.1. Test rig types

Taking into account of the references from literature, the main test rig types for gear testing are:

1. Mechanical test rig, open circuit;
2. Electrical test rig, open circuit;
3. Mechanical test rig, closed circuit;
4. Electrical test rig, closed circuit.

Below will be analyzed few representative types of test rig designed to test cylindrical gears. Bibliographic stydy shows that most utilized test rigs are mechanical with closed circuit, so these will be presented below.

Most popular loading systems are shown in Chironis (1967).

2.3.2. Actual stage for experimental research

Upon the studies of **Khang, Cau și Dien, (2004)**, the main components in gears vibration are meshng frequency and its harmonics, along with subarmonics due to modulation effect. Subharmonics could be used as diadnistic element in gears failure. Parametric excitation of gear mesh was studiedand a comparison between model and test rig experiment was realized. The fenomenology was later explained via analitical expressions. The test rig used by authors is depicted in picture 2.19.

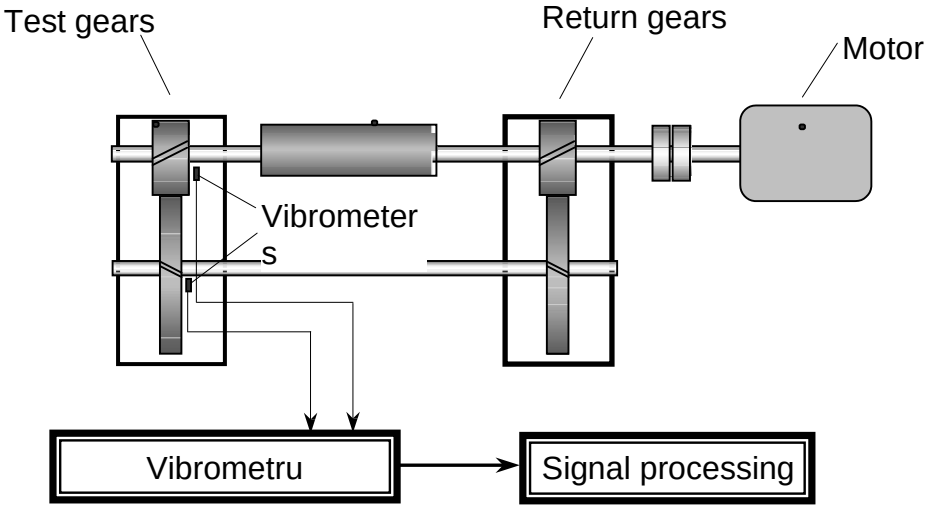

Picture 2.9. Test rig for identification of defects effect on the gear operation, (Khang, Cau and Dien, 2004)

Other paper **(Hargreaves, Planitz, 2008)** describes the componence and

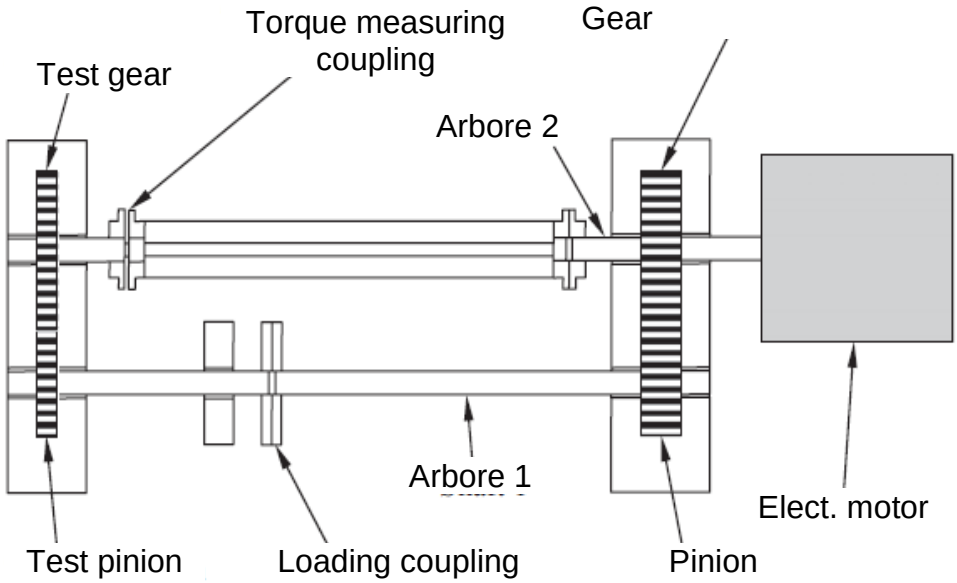

Picture 2.10. FZG type test rig, closed circuit (Hargreaves, Planitz, 2008)

operation of a FZG-type test rig, depicted in picture 2.10. Test gears being high precision, lubrication efficiency testing is relevant, too.This test rig is designed to evaluate oil quality, too.

Davali, Garla, Rosa și Boni (2007) studied the total error problem og the gear mesh, using as measurable parameter the operating noise. Picture 2.11 depicts the test rig used. The construction is simple, open circuit.

The conclusion of the bibliographic study is that in almost all cases, for gears testing closed circuit test rigs are to be used.

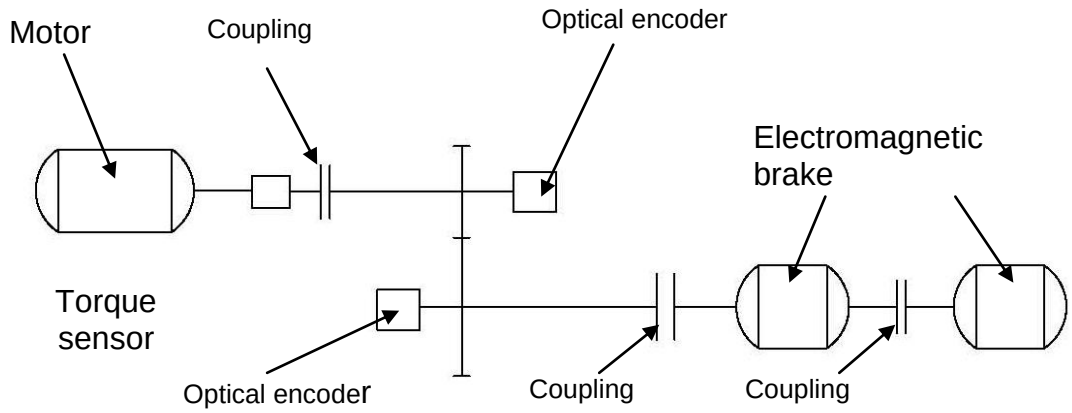

Picture 2.11. Total gear meshing error identification test rig (Davali, Garla, Rosa and Boni 2007)

A high power test rig, aimed to test meshing gears for pitting, scuffing and scoring was designed and built by INCDT-COMOTI, under European research contract ESPOSA, WP 3.4. This test rig tests special design gears, based upon the expertize of one of the partners, P&W of Canada.
Picture 2.12 presents the test rig and the componence of the installation is presented in picture 2.13, operating parameters being contained by table 2.3.

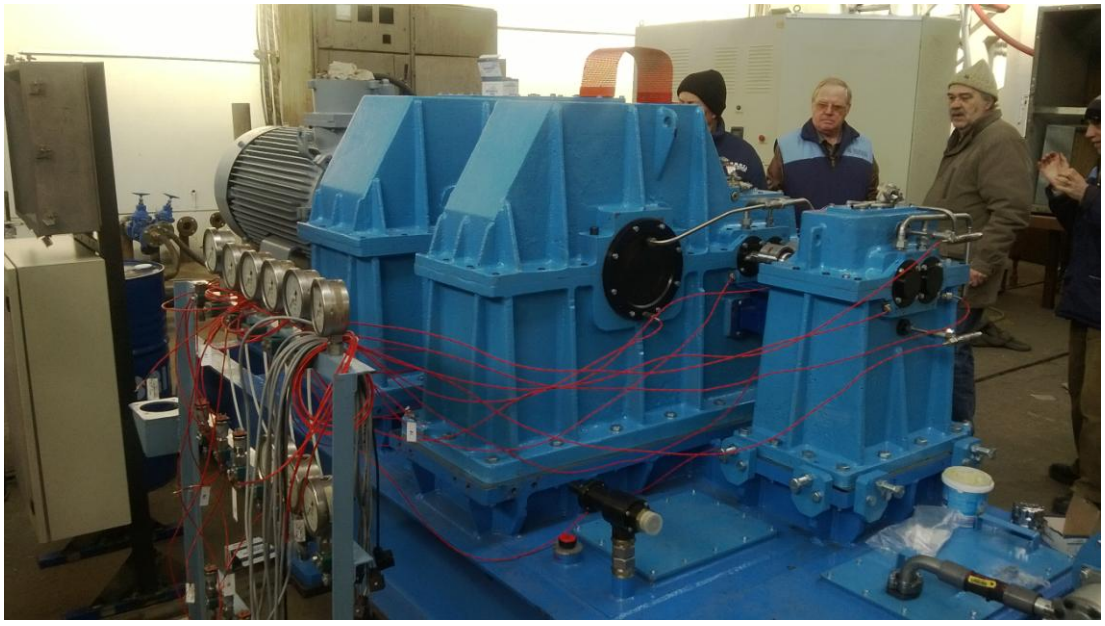

Picture 2.12. ESPOSA – INCDT-COMOTI test rig, (upon Gabroveanu, 2016)

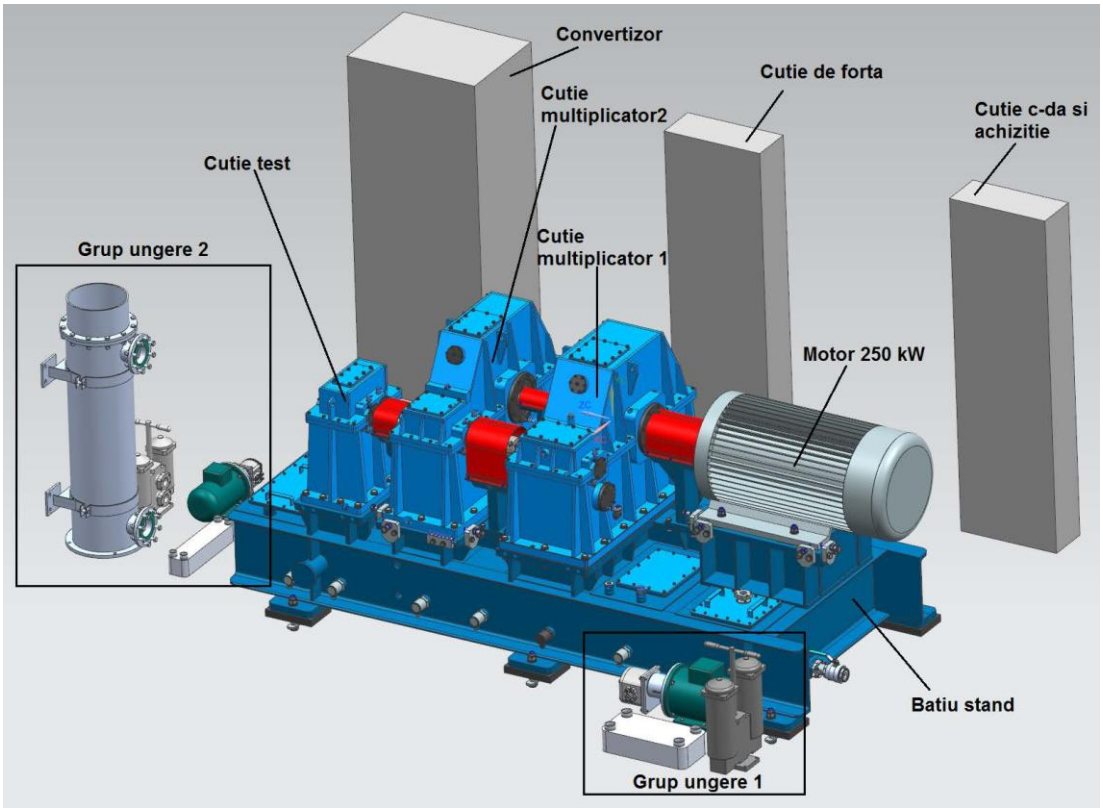

Picture 2.13. ESPOSA test rig componence INCDT-COMOTI (upon Gabroveanu, 2016)

Table 2.3

Parameter	Limits	Obs.
Speed	300 – 20000 RPM	
Torque	10 – 500 Nm	Variable in operation
Oil temperature	15 – 120 C	
Oil flow	1.2 – 30 l/min	Variable in operation

2.4. Research directions required for thesis finalization

Taking into account the actual status presented before, following directions for research could be formulated, by scope and objectives.

Scope. Present paper study the influence of gradului de acoperire suplimentar on the vibroacoustic behaviour of meshing gears, based on the fact that there are required even more researches in completion of the actual status.Theoretic and experimental research methods will be proposed, able to produce results of interest for practical applications.

Objectives required to fullfill the scope are listed below:

a) Theoretical studies based on FEA method, applied on different meshing gears and ways to apply the method: meshing,

discretization, elements desities in network, boundary conditions, result interpretation etc.Using this way can be studied the meshing stiffness in different points on action line.

1. Experimental research:
   a) Static and dynamic test rig proposal;
   b) Experimental research on meshing stiffness;
   c) Experimental results;
   d) Result comparison with own theoretical results.

By the way, the scope and objectives of the whole paper can be fulfilled, as enounced in subchapter 1.2.

3. RESEARCHES AND THEORETICAL CONTRIBUTIONS

3.1. Scope and objectives of the theoretic research

Theoretic research scope mainly is to simulate, using mathematical ways the meshing process.

We can see two simulation directions to simulate these phenomenons, more precisely:

- Static simulation of the meshing, seen as a succesion of positions, treated separately, meaning a point by point approach;
- Dynamic simulation of the meshing process.

Both simulation types, uses finite elements discretization, an well known method and widely used to simulate different processes.

Present paper emphasises the statis stiffness testing, as an alternative ti huge FEA models, requiring high capacity computing systems.

Using FEA method was possible to simulate static meshing, stiffness values being obtained for every considered point on the action line.

3.2. Theoretical research using FEA method

3.2.1. Basic concepts in finite element analysis

Few basic concepts used in FEA method are listed below.

1. Structure. Assembly of solid volumes, interconnected, working as an unit.

2. Computational model. The FEA model is a mathematic representation of the structure to be simulated.

3. Discretization. Represents the action making the passage from a continuous model to discrete structure, with finite point number.

4. The node. The points of the discrete network are named nodes. Here are defined the primary unknown values, displacemets or tensions.

5. Finite element. Appears following the discretization – the division of the structure in small fragments, linked via common nodes.

3.2.2. Gear meshing characteristic parameters studied using finite element method

3.2.2.1. Finite element analysis steps

The analysis steps are:

1. Main data of the gears, required by FEA study;
2. Discretized meshing gears models;
3. Boundary conditions;
4. Putting the model in specific position, corresponding to A, B, C and so on;
5. Contacts declaration;
6. Numerical solving of the model;
7. Specific calculations, producing mesh stiffness values.

3.2.2.2. Meshing gears data

Evoventic meshing gears studied was elected in ideea to have overlap parameter natural number. Experiments being required, was chosen the variant with $\varepsilon_\beta = 1$. Meshing gears with overlap parameter inferior to the unit will be subject of experiment, too, to see the variation trend in such cases.

Main data for this meshing gears are indicated in table 3.1.

Table 3.1.

Name	Symbol	Value
Distance between axles	a_w	125 mm
Pinion teeth number	z_1	15
Gear teeth number	z_2	46
Helix angle	β	10°
Profile shift coefficient for pinion	x_1	0.427
Profile shift coefficient for gear	x_2	-0.138
Gear width	b	72.3668 mm
Transverse overlap factor	ϵ_α	1.45318
Supplementary overlap factor	ϵ_β	1
Basic torque, pinion	T_1	392.466 Nm

Basic applied torque was established using resistence of the gears to root bending and contact fatigue, upon ISO-3 6336:2006 şi ISO-2 6336:2006).

Must be mentioned that the studies were performed using other loads, too, to reveal the influence on other parameters, via FEA analysis.

3.2.3.4 Meshing gears modeled

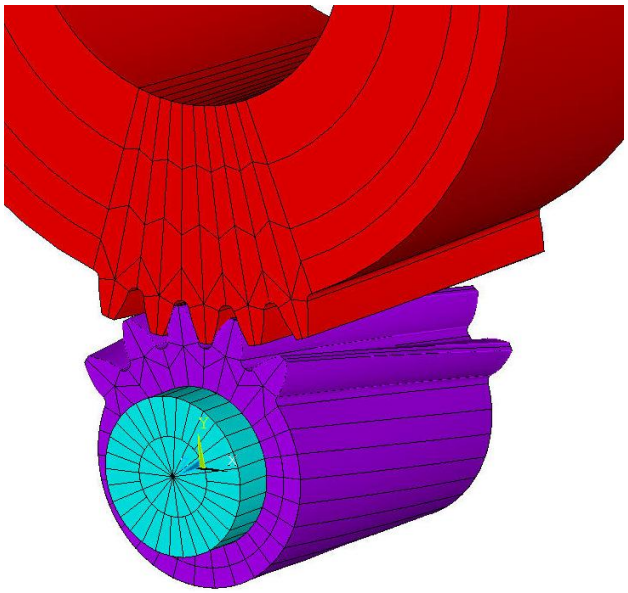

Figura 3.1. Finite element model of the (Dobre, Mirică, Gabroveanu, 2008)

The detailed mesh that will be referred to regarding the method used is shown in fig. 3.1, with the applied torque being $0.5T_1$, $0.75T_1$ and T_1;

To conserve space, only five gear teeth have been modelled in both the driving and the driven gear.

The 3D mesh is generated automatically after setting up the meshing parameters.

The contact elements are automatically generated by the analysis program. The resulting models discussed in this paper take up in excess of 16 GB using ANSYS. Use of other analysis programs can lead to the creation of even larger buffer files.

3.2.2.4. Boundary conditions

Figure 3.3 displays the boundary conditions applied to all meshing

The applied boundary conditions are shown in figure 3.3 (for all meshing positions). The torque labelled T_1 is applied to all meshing positions in the shaft area (30mm diameter). While the driven gear borehole area is fixed rigidly(50mm diameter), both the driven and the driving gear OZ axis deformation is possible (much smaller displacement than elastic rotation displacement), with only the “rear” area being fixed. The driving gear shaft axis bending is also suppressed. Gearing is subjected to shaft bending in real use scenarios, so additional displacements may exist.

3.2.2.5. FEM model positioning

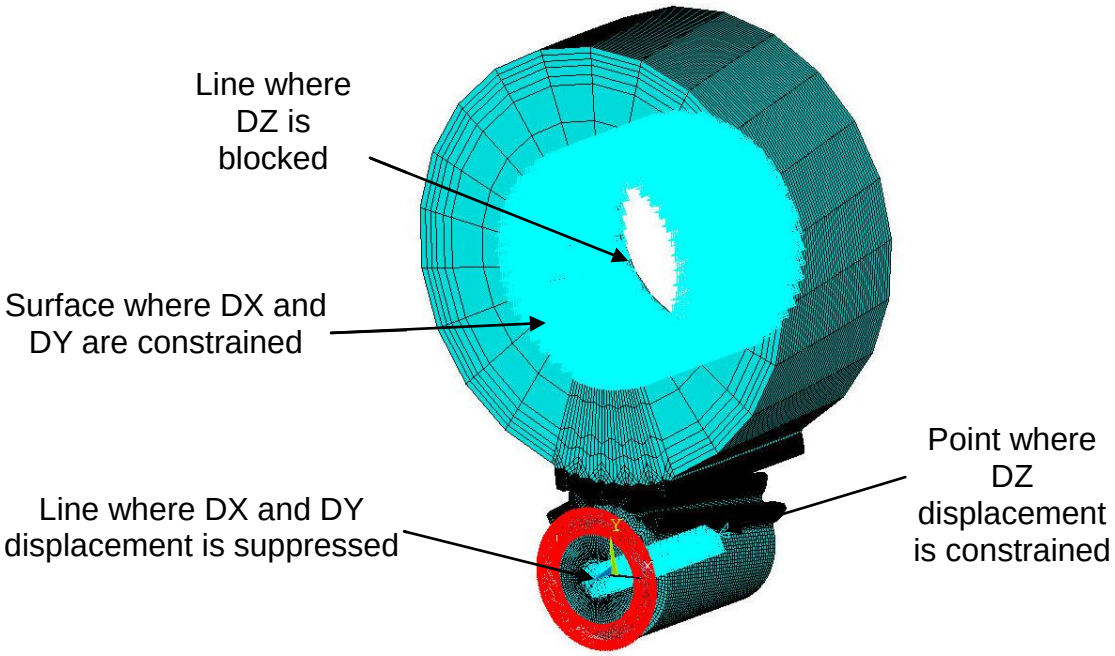

Figura 3.3. FEM boundary conditions (Dobre, Gabroveanu, Mirică, 2008)

The model is analysed in meshing points(the main ones are shown in figure 3.4) . The distance between these points and point A,the theoretical meshing initiation point, is displayed in table 3.3 (which indicates other elements studied to be referred to later) .

Tabelul 3.3. Characteristic meshing points

Point	Distance on contact line [mm]	Maximum penetration [μm]
A	0	2.75
1	0.7125	2.89
2	3.2194	2.87
3	5.2182	2.11
B	5.4244	4.18
4	5.9166	3.36
C	6.5465	2.19
5	8.7186	3.74
6	11.2165	2.75
D	11.9689	2.75
7	14.7169	2.67
8	16.2172	2.24
E	17.3933	2.75

Positioning the gears in these characteristic points is achieved by rotating each gear by the suitable angles measured between the gear centerline and the gear tooth symmetry axis which is rotated

3.2.2.6. Contact setup

This stage requires that the second stage be finalized by bringing the model into the right position. The program used, ANSYS, includes a special module for setting up contacts.

Initial penetration owing to the imprecise nature of the surface mesh is present upon bringing the surfaces into contact. Figure 3.4 displays the surfaces corresponding to one of the cases studied.

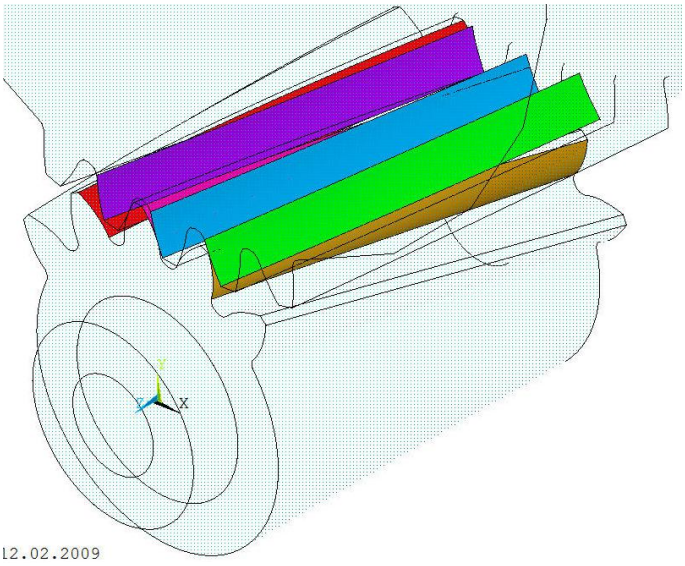

Figura 3.4. Suprafețe de contact (colorate diferit) în poziţia de angrenare C

3.2.2.7. Rezolvarea numerică a modelului

From a mathematical standpoint, the finite element method is an approximate method used to solve partial differential equations used to describe given physical phenomena. This method can be applied to virtually any domain where phenomena can be described by differential equations. From a mathematical point of view, the problem is described by a set of partial differential equations ,as well as boundary conditions resulting from the particular case studied.

3.2.2.8. Meshing stiffness computation tehcnique

Defining meshing stiffness has proven to be a difficult issue when usint the finite element method. As shown in Dobre, Gabroveanu and Mirică (2008), based on the defined boundary conditions and using the notation in figure 3.5, the following conclusion can be reached:

1. tangential displacement u_t is quasi-linear in the transversal plane, from the shaft axis to the gearing root diameter;
2. Assuming quasi-linear tangential displacement along the measuring circle of diameter d_c is relatively small compared to the gear radius, the relative rotation angle is approximately:

$$\varphi_{12} = \frac{2\,u_t}{d_c}; \tag{3.14}$$

3. average tangential displacement is:

$$u_{t\,m} = \frac{\oint_A u_t \, dA}{\oint_A dA} = \frac{\oint_A u_t \, dA}{\pi \, d_c \, b}, \tag{3.15}$$

where dA is the area element on the lateral surface of the cylinder;

4. The average relative angular displacement , using 3.14, is:

$$\varphi_{12\,m} = \frac{2\,u_{t\,m}}{d_c}; \tag{3.16}$$

5. meshing stiffness can be expressed as:

$$k_{t\,m} = \frac{T_1}{\varphi_{12\,m}}. \tag{3.17}$$

Several considerations concerning the models are:

- each FEM model was run (solved) in points A,B,C,D,E on the contact line, as well as the additional points 1, 2, 3, 4, 5, 6, 7, 8;
- Computations were run for three values of applied torque, 50%, 75% and 100% of the rated torque for each point on the contact line.

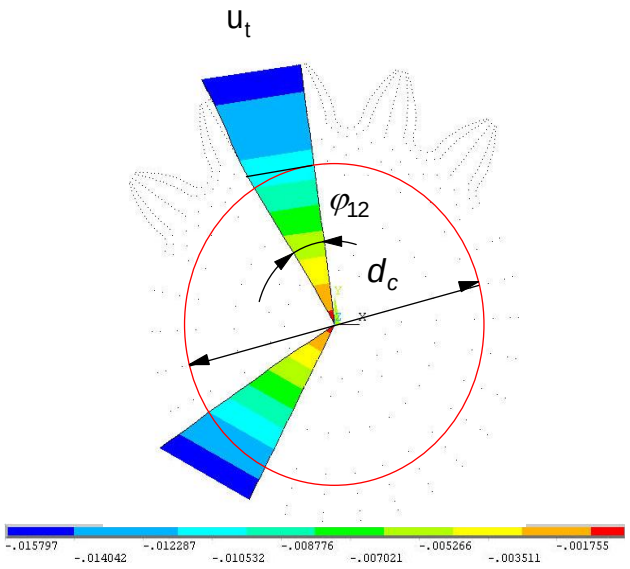

Figura 3.5. Tangential displacement in transversal section, gear tooth midplane (Dobre, Gabroveanu, Mirică, 2008)

3.2.3. Results obtained

3.2.3.1. Meshing stiffness

1. The maximum penetration is approximately 4 micrometers, encountered in regions where larger values of the contact pressure are, generally at the gear tooth tip. Taking into account that the average roughness is approximately equal to 2 micrometers in the case of ground gear tooth face, the resulting precision is acceptable.

2. The contact lines are visible only in the figure displaying the contact pressures, as displacement values are too low to be discernible in figure 3.4.

- gearing contact forces are constant (invariant) for all meshing positions; in the global reference system : **F_x = 12766 N; F_y = 5064 N şi F_z = 2272 N**.
- the contact surface length is constant, circa 1.5 B (B is the gear width).
- torsional stiffness $k_t = \frac{M_t}{\varphi_{12}}$ is, in the gearing midplane(only for the applied torque, owing to the fact that displacement is nonlinear) is about 700 kNm/rad and is approximately equal in all meshing position cases ($\varphi_{12} \cong \frac{0.015}{27.17}$ rad = 0.03 degrees, transversal displacement at the gear tooth base divided by the tooth base radius). The fact that the torsional stiffness is aproximately constant also stems from the total displacement field analysis in the five meshing positions, with varying between 0.02228 (min pos. D) and 0.02367 (max pos. E).

-the resulting computation penetration (below 1 micrometer with maximum values under 4 μm) as well as geometry approximation errors are considered acceptable from a FEA standpoint.

-Stress distribution computation accuracy is acceptable, although the contact zone mesh should be refined.

Observation: the elastic circumferential displacement showed in figure 3.8 varies in a linear fashion to the tooth root region, hence any cylinder with a diameter satisfying this condition can be used to define relative angular displacement. A reference diamater of 40 mm was selected. The relative angular displacement is:

$$\varphi_{12} = \frac{\int_0^b \int_0^{2\pi} \upsilon(\theta, z)\, d\theta\, dz}{\pi\, d_m\, b} \qquad (218)$$

Figure 3.11 displays the results obtained.

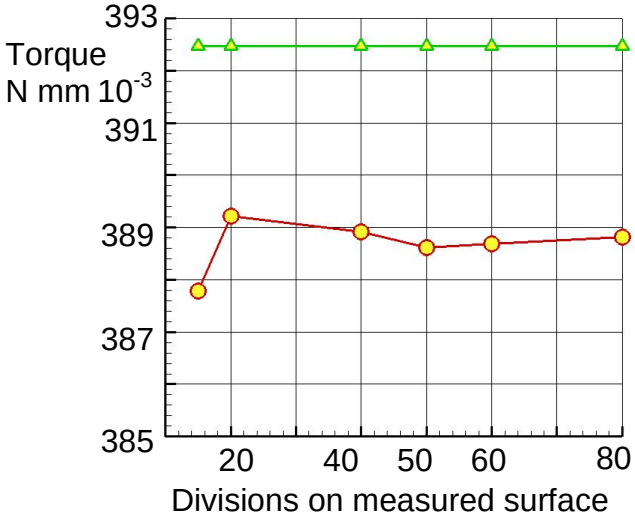

Figure 3.9. torque variation as a function of surface mesh size

3.2.3.2. Additional results

Figure 3.9 highlights one of the problems encountered in finite element modelling, that is the applied torque computation error or, more accurately, the resistive torque. It is noticeable that,

if the measured surface mesh is courser, this will affect the results. The interesting theme is that calibration is necessary for every model or model family.

Figure 3.10 shows the integration surface for torque and displacement.

3.2.4 Method limitations and possible corrections

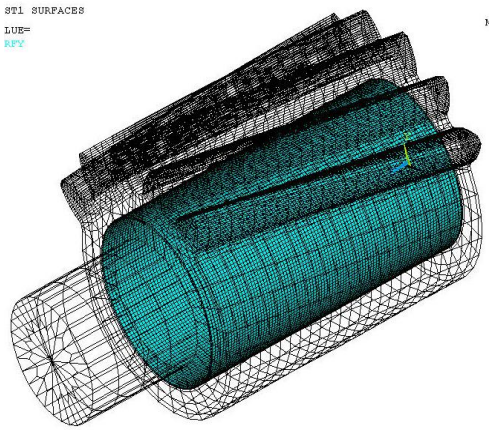

Figura 3.10. Cyllindrical torque and displacement integration surface

The following observations can be made:

1. the model must and will be improved, with error curves being traced to establish optimum mesh density.
2. final validation of the model requires experimentally based corrections in order to evince all displacement of the parts in contact.

Table 3.3 contains the computation results

Table 3.3. Computation results

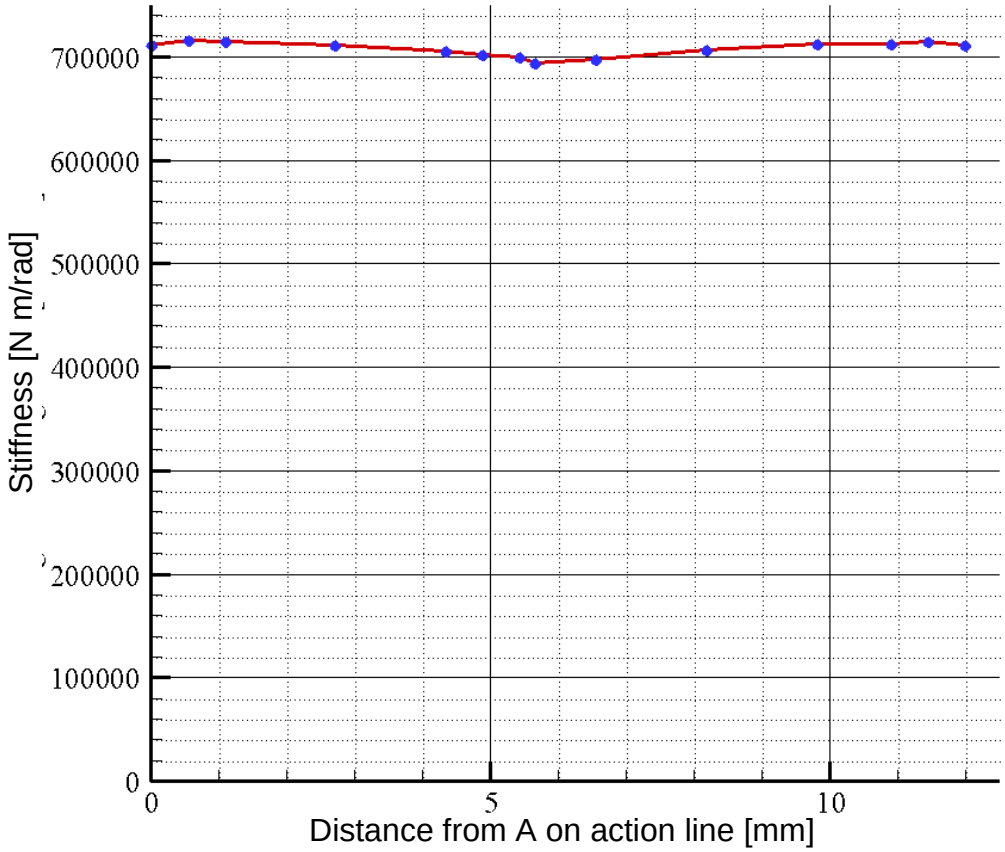

Fig. 3.11. Static mesh stiffness along the action line, averaged over the 40 mm diameter cylinder.

Point on contact line	Distance along action line from point A [mm]	Maximum Hertzian displacement Maximum penetration [μm]	Average relative angular displacement in the front view plane where torque is applied [rad]	Meshing stiffness $\cdot 10^3$ [Nm/rad]
A	0	2.75	$551.52 \cdot 10^{-6}$	711.61
1	0.54242	2.89	$548.63 \cdot 10^{-6}$	715.36
2	1.08483	2.87	$548.91 \cdot 10^{-6}$	714.99
3	2.71207	2.11	$551.46 \cdot 10^{-6}$	711.68
4	4.33930	3.36	$556.46 \cdot 10^{-6}$	705.29
5	4.88172	3.74	$558.94 \cdot 10^{-6}$	702.16
B	5.42416	4.18	$560.72 \cdot 10^{-6}$	699.92
6	5.64856	2.75	$565.84 \cdot 10^{-6}$	693.60
C	6.54616	2.19	$562.91 \cdot 10^{-6}$	697.21
7	8.17306	2.67	$555.74 \cdot 10^{-6}$	706.20
8	9.79986	2.24	$550.84 \cdot 10^{-6}$	712.48
9	10.88436	2.07	$550.71 \cdot 10^{-6}$	712.66
10	11.42666	2.44	$549.00 \cdot 10^{-6}$	714.87
D	11.96896	2.75	$551.44 \cdot 10^{-6}$	711.70

3.2.4.1. Conclusion

The sole conclusion is that the finite element method confirms the hypotheses of quasiconstancy of meshing stiffness if the overlap is a natural number.

As an active measure of reducing source vibration in gearing, aside from the widely studied profile correction, the reduction of mesh stiffness appears to be a very promising solution.

The practical advantage is that this can be easily applied to turbotransmission, where wide gearing is used and where, for this exact reason, it is very difficult to realize profile correction.

The gearing studied is included in this category, the Finite Element Method study demonstrating the following points:

1. Irrespective of the computation premise, mesh stiffness variation is small, under 3%.
2. The hypothesis taking into account the full width of the gearing is a good approximation of reality, but an experimental stage is required to achieve complete certainty.
3. In the studied cases, mesh stiffness is smooth, without sudden jumps.

3.3. Theoretical research on dynamic mesh simulation using the specialized software MSC ADAMS 2015.1

3.3.1. Studied gearing

Two versions of gearing were examined, with two specified gearing widths as shown in table 3.4. When width is equal to 72.3668 the overlap is equal to the unit, whereas when width is 62.3668 the overlap becomes 0.8667.

Table 3.4

Name	Symbol	Value
Distance between axes	a_w	125 mm
Driving gear tooth number	z_1	15
Driven gear tooth number	z_2	46
Helix angle	β	10°
Driving gear normal profile displacement coefficient	x_1	0.427
Driven gear normal profile displacement coefficient	x_2	-0.138
Gear width	b	72.3668/68.3668 mm
Transversal contact ratio	ϵ_α	1.45318
overlap	ϵ_β	1/0.8667
Base torsional moment applied to driving gear	T_1	392.466 Nm

The large width gearing will henceforth be referred to as the wide gearing, while the small width gearing will be referred to as narrow gearing.

3.3.2. Meshing simulation

3.3.2.1. Simulation conditions

The operation of the two gearings, wide and narrow , was simulated under the following conditions:

1) Constant driving gear angular velocity, n=1000 RPM, 2000 RPM, 3000 RPM;
2) Applied torques of values: 100 Nmm, 100000 Nmm, 200000 Nmm, 300000 Nmm, 280000 Nmm, 320000 Nmm;

Table 3.5 contains the simulation data for each case.

Table 3.5

N1, RPM	Duration, s	Step, s	Number of complete rotations	Angular velocity, deg/s
1000	0.1	0.0001	1.67	6000
2000	0.050	0.00005	1.67	12000
3000	0.0334	0.0000334	1.67	18000

3.3.3 Results

3.3.3.1. Narrow gearing, 0.8667 overlap

The angular velocity and angular acceleration diagram has been included for each driven gear analysis case.

3.3.3.2. Wide gearing, 1.0000 overlap

The angular velocity and angular acceleration diagram has been included for each driven gear analysis case.

3.3.4 Comparative study of the two gearing types

3.3.4.1 Results summary

3.3.5 Interpretation of results

Comparing the angluar velocity RMS values makes sense. It can be seen that the ratio of the two RMS values at the same loading clearly favors the gearing where the overlap is equal to the unit (the wide gearing). Figure 3.12 displays the variation of angular acceleration as a function of applied torque at a driving gear speed of 1000 RPM, figure 3.13 at 2000 RPM and figure 3.14 at 3000 RPM.

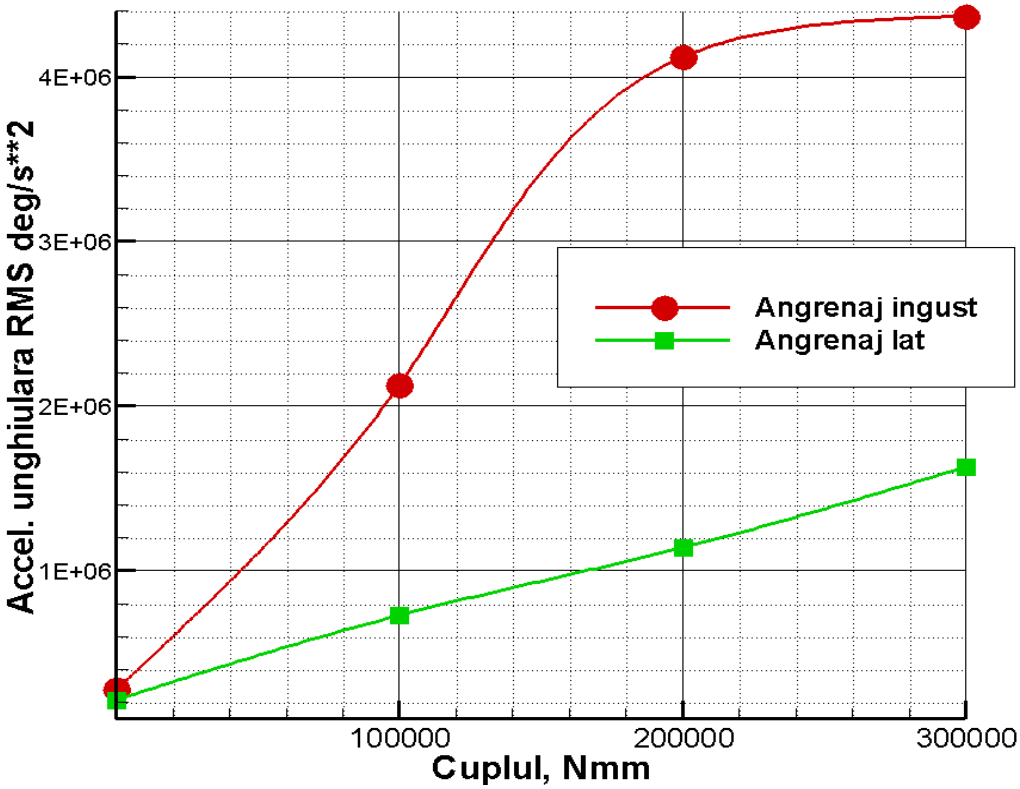

Fig. 3.12.Driven gear RMS angular acceleration at 1000 RPM driving gear speed.

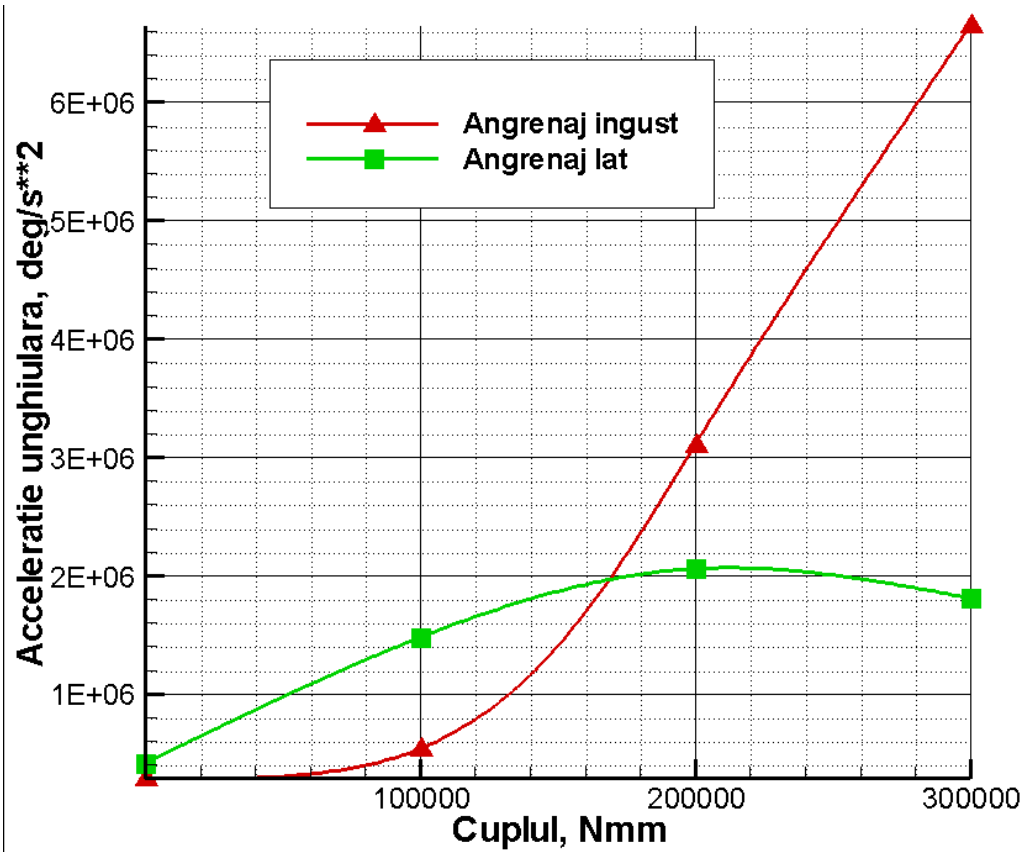

Fig. 3.13 Driven gear RMS angular acceleration at 2000 RPM driving gear

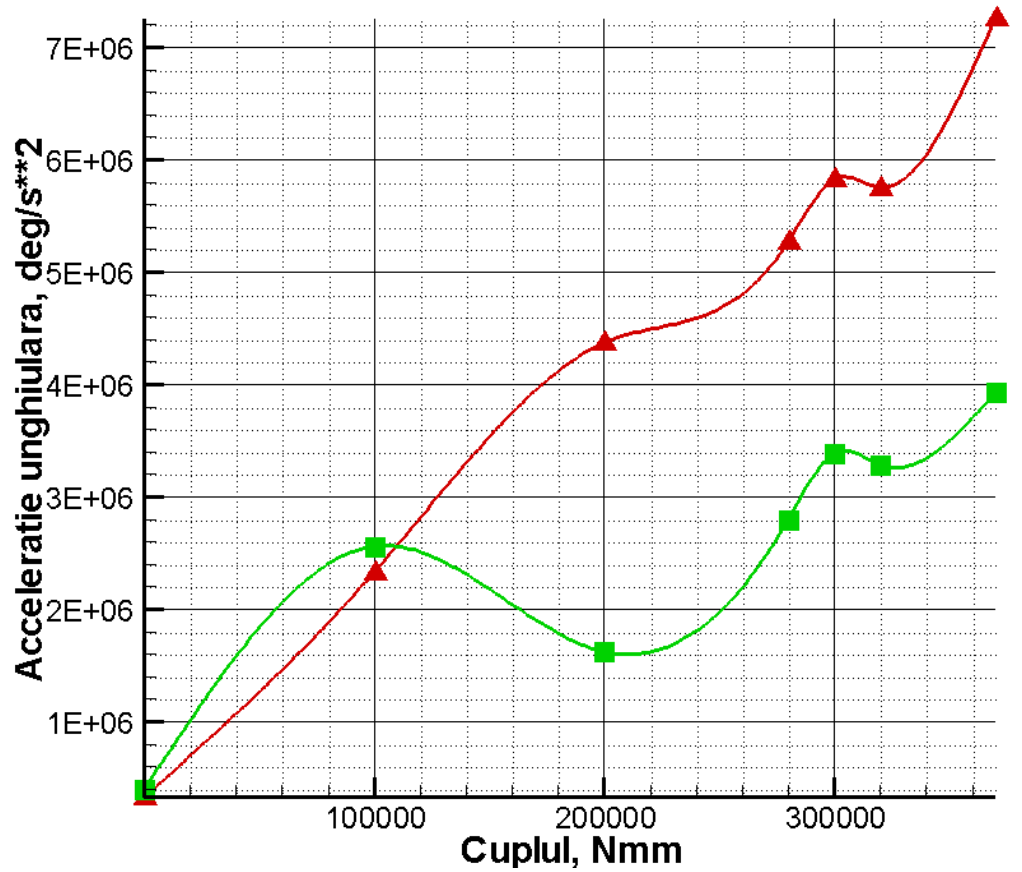

Fig. 3.14 Driven gear RMS angular acceleration at 3000 RPM driving gear

3.3.6 Conclusion

The gearing is designed to function at torques in excess of 200000 Nmm, the computation point being 392000 Nmm.

According to figures 3.12 – 2.14, the driven gear angular acceleration in the wide gearing case is clearly to the narrow gearing (overlap is less than one)

3.4 General conclusion of theoretical research

It was postulated that a gearing with low intensity internal excitation sources will experience reduced vibration in operation.

The main internal excitation source is the mesh stiffness variation.

The finite element method demonstrates that a gearing with unit overlap experiences vastly reduced stiffness variation compared to the results presented in References.

It has been demonstrated theoretically by the means of direct simulation that gearings with contact ratios equal to the unit exhibit more stable operation where vibration is concerned.

4. ORIGINAL RESEARCH AND EXPERIMENTAL CONTRIBUTION

4.1. Test rigs

4.1.1. Static test rig for meshing stiffness measurement

4.1.1.1. Rig description

As shown in figure 4.1, the static meshing stiffness measurement test rig is a simple rig, perfectible and easy to use.

The measuring systems used include a laser pointer affixed to the driving gear, as well as a high accuracy load cell.

The load cell also fixes the driving gear on the axis direction, preventing displacement in this direction.

It was observed that as work with the rig progressed, modifications were operated by means of simplification of certain aspects and by increasing the complexity of others.

Research was carried out using a test rig of original construction, ensuring the application of various torques in the 0-400 Nm interval.

The rig ensures the positioning of the two gearing components at the correct angles.

The unit overlap gearing has been used for testing at multiple values of the applied torque. The values of angular displacement were measured during each test in order to enable the computation of the meshing stiffness.

4.1.1.2. Method used

A key element is the meshing stiffness measurement in the characteristic positions along the contact line.These values were computed using the finite

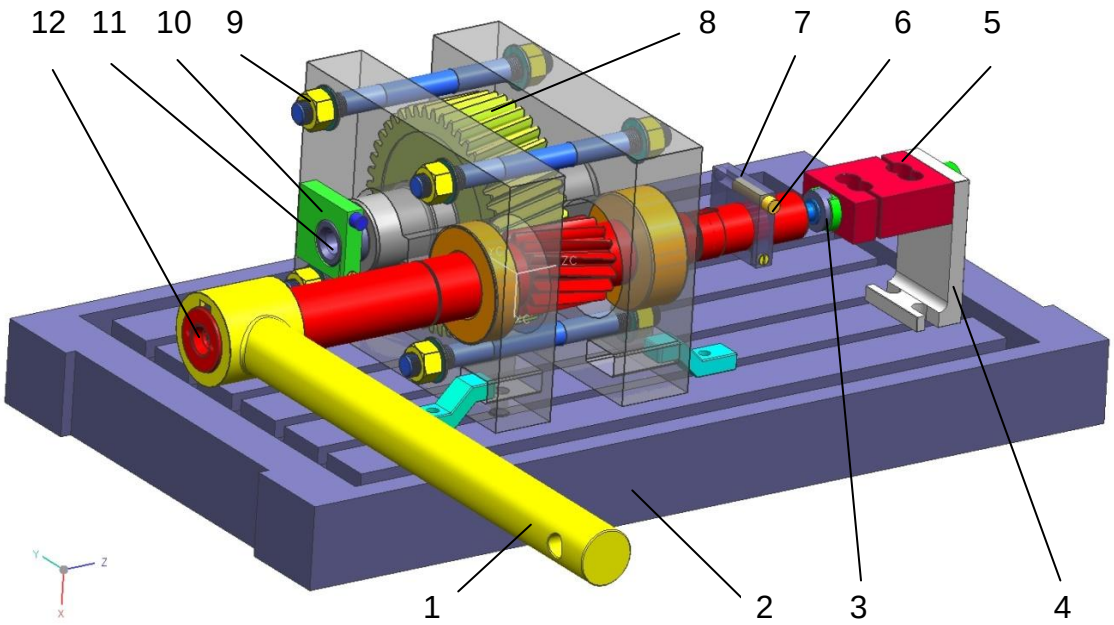

Figura 4.1. Static meshing stiffness test rig (Gabroveanu, Tudor, Cananau and Mirică, 2015)

1. loading arm; 2. support structure; 3. axial ball bearing; 4. brace; 5. load cell; 6. driving gear laser pointer; 7. laser pointer holder; 8. driven gear; 9. stud; 10. driven gear laser pointer; 11. arbore

element method in three distinct load cases which were also simulated using the test rig.The experimental installation is displayed in fig. 4.1.

The rig is meant to solve the problem of angular displacement measurement when the driving gear is loaded in contact with the driven gear. Load application is done easily, through the application of weights with strain gauge control of the applied load. The driving gear is free to rotate around its axis under the effect.After this stage, the angular displacement between the tooth contact position and the rest position of the driving gear will be measured. Another problem that needed to be solved was that of the angular displacement under load measurement accuracy. The measurement of this angle is done optically due to the numerous benefits of this method. The axial displacement of the driving gear is limited by the axial load cell, coupled with the driving gear by the axial ball bearing. The system registers reduced friction due to the use of ball bearings. The system friction can be estimated using the two coupled measurement systems, the strain gauge on the load application arm and the axial force load cell.

The measurement accuracy is ensured using a medium power laser, which ensures ease of reading when the measurement screen is positioned at least fifty metres away.

The solution selected here makes use of laser pointers to measure the assembly displacement in a direct experimental fashion. In order to ensure the assembly mesh stiffness, a T-channel machine tool table was used, preserving its original positioning mechanism. Ball bearings were used for the driving gear, while the driven gear features a classical bearing solution, shaft and bushing. The driving gear is free to rotate with the loaded assembly beaing stabilized by constraining the driving gear axially (by the use of a load cell which also serves to verify the rig status). The method applied guarantees positioning accuracy superior to all other methods, given that the measurement surface can be placed at considerable distance.

Considering the fact that the laser pointer center is always used for positioning and the minimum perceived distance between the dot positions is 0.5mm, the angular resolution values are as shown in table 4.1 at different placement radii of the measurement screen.

Tabel 4.1. Measurement angle accuracy

Radius [m]	Angular accuracy [seconds]
2.00	51.5
4.00	25.8
6.00	17.2
8.00	12.9
12.00	8.6
15.00	6.9
60.00	1.71

The system used to read displacement relies on the movement of a laser pointer. TO obtain good measurement accuracy, a large distance to the measurement screen is advisable, but this poses problems due to the laser beam dispersion. Thus a compromise is needed, which implies that it is possible to read the dot position on a screen 13.5 m away with a 0.1 mm accuracy. By making improvements to the laser pointer focus, the distance will increase, as will the accuracy. The same advancements can be obtained through the use of high power laser, although this is difficult to obtain and is very dangerous to use in areas with numerous parasitic reflections. The measurement procedure is described below:

1. the loading arm is aligned horizontally. This is done using a bobble level or electronically;
2. the driven gear is brought to the meshing position using the corresponding centering (?? calibru ??) (A,B,C,D,E);
3. the nuts are tightened in a cross pattern until the gear is fixed;
4. the loads are applied recording the deflection angles of the free end of the driving gear;

5. the values shown by the load cell is registered at the same time.

   The loading conditions have been realized using a three step loading scheme with a maximum of 78 daN.

   The loading data is showh in table 4.3.

Tabel 4.3. Static rig loading data

Load step	Applied load [daN]	Driving gear applied torque [Nm]
1	39	195
2	58.5	292.5
3	78	390

The distance to the measurement screen was 60 m.

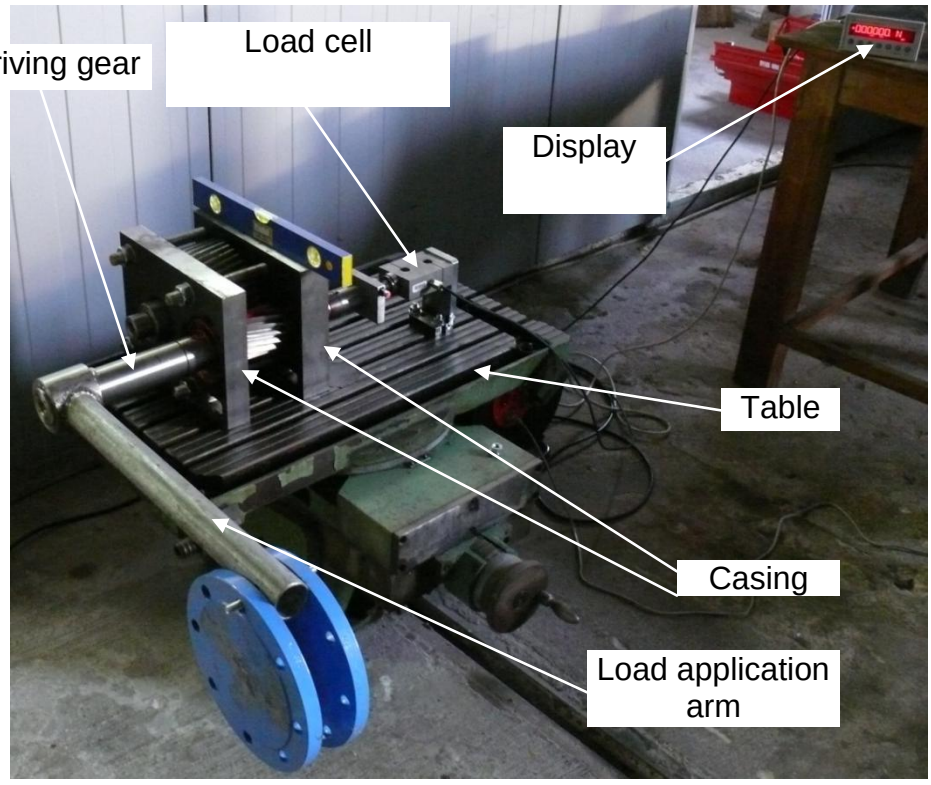

Figura 4.3. The static mesh stiffness rig general assembly, also showing instruments.

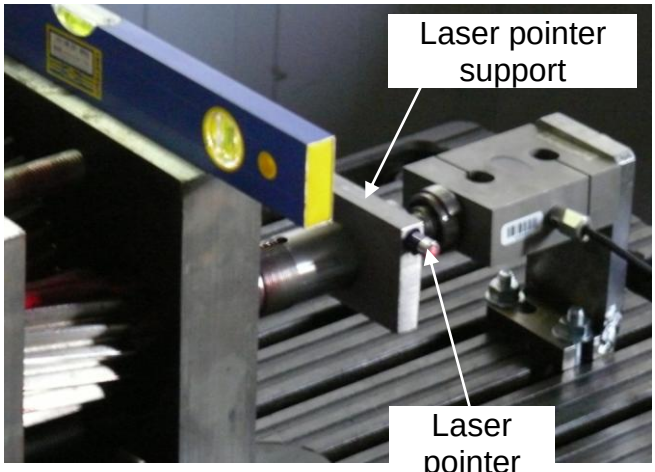

Fig.4.4. Part of the static mesh stiffness test rig snowing instruments.

4.1.2. Dynamic test rig for the study of vibration behaviour

4.1.2.2. Rig description

Evaluating both vibration behaviour as well as load distribution on the number of tooth pairs is done using a closed-circuit dynamic mechanical test rig, as shown in figure 4.6

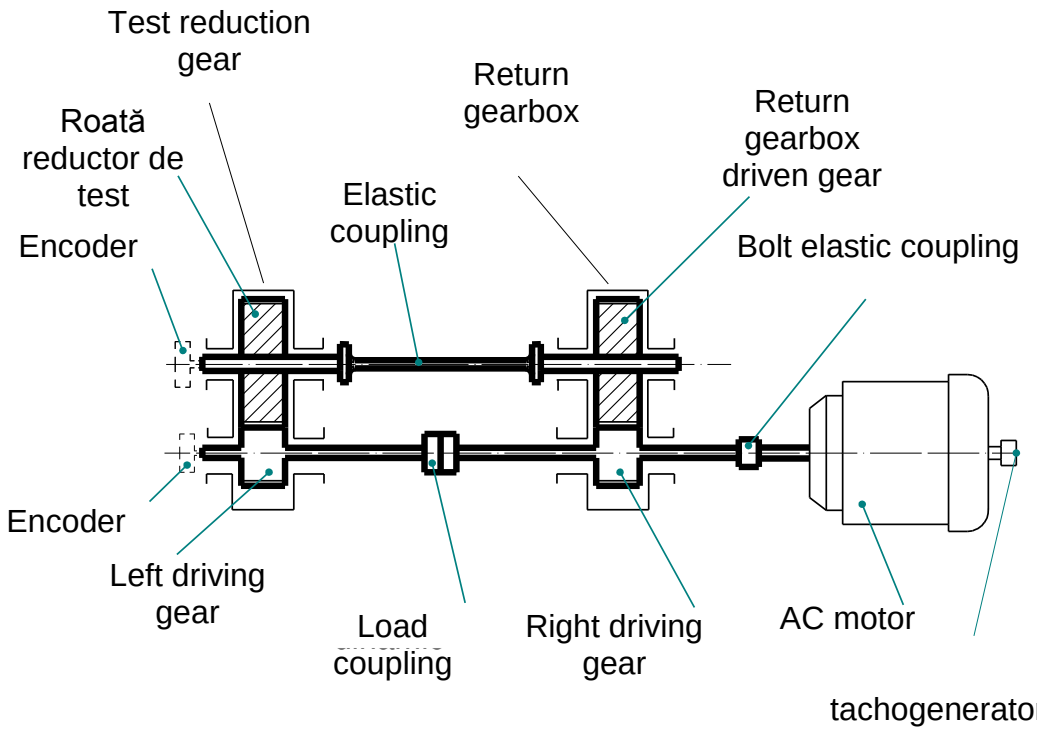

Figure 4.5. Dynamic test rig drawing (Gabroveanu, Tudor, Cănănău și Mirică, 2015)

Thus, multiple series of experiments have been carried out using this test rig, differing by:

- different widths of the studied gearings;
- different loading of the studied gearings;
- different velocities for the tests carried out.

The transmission is loaded through the shafts end shifting applied to the shaft ends by using the loading coupling.The applied torque is measured using a strain gauge included in the elastic coupling. Signal reception

from this strain gauge is provided by an HBM SK 6 type sliding contact block.

The test rig is equipped with the following instruments:

1 precision optical encoder type ROC 425 produced by Heidenhain Germany, 2 devices;
2 T10FS Hottinger Baldwin Messtechnik contactless torque transducer, 0,05% precision;
3 temperature data aquisition lines for oil temperature in the reduction gearing oil baths for both the test and the return reduction gear.,
4 AC motor rotational velocity measurement,
5 general rig vibration level- Bentley-Nevada data aquisition lines.

The Heidenhain ROC425 optical encoders are used to measure torsional vibration. Encoders of this type are designed to work together through a dedicated data aquisition board manufactured by the same company.

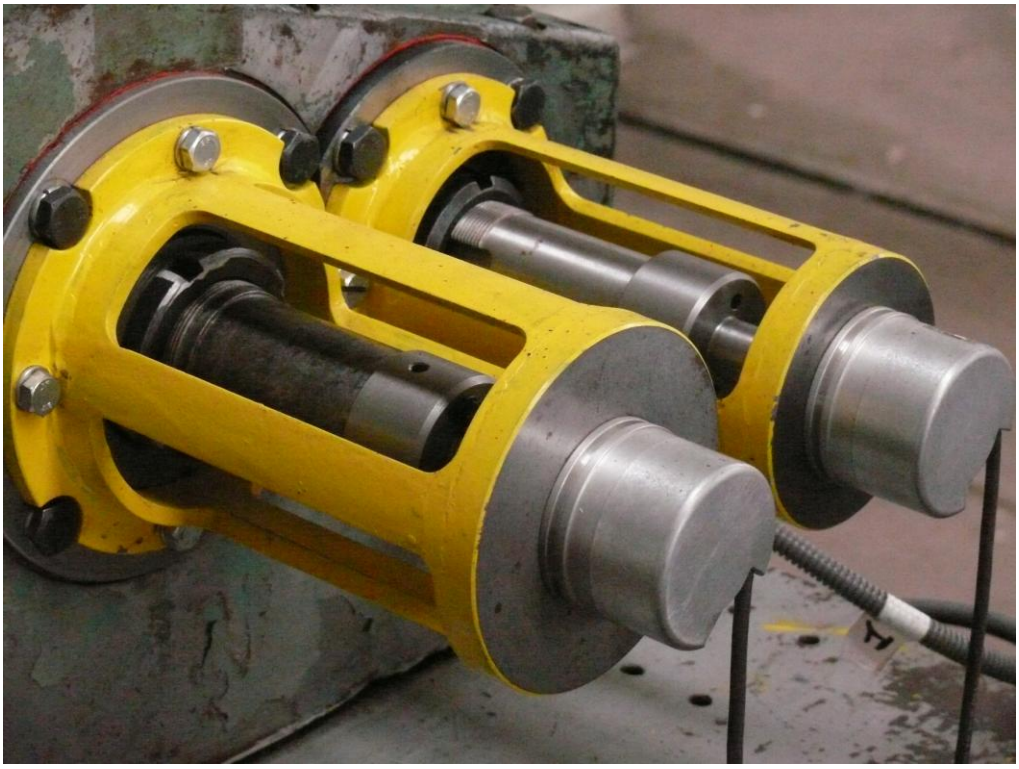

Figure4.6. Heidenhain ROC 425 optical transducer detail view

Figure 4.7. Temperature, vibration and speed control PLC

Figure 4.8. Bently Nevada vibration transducer

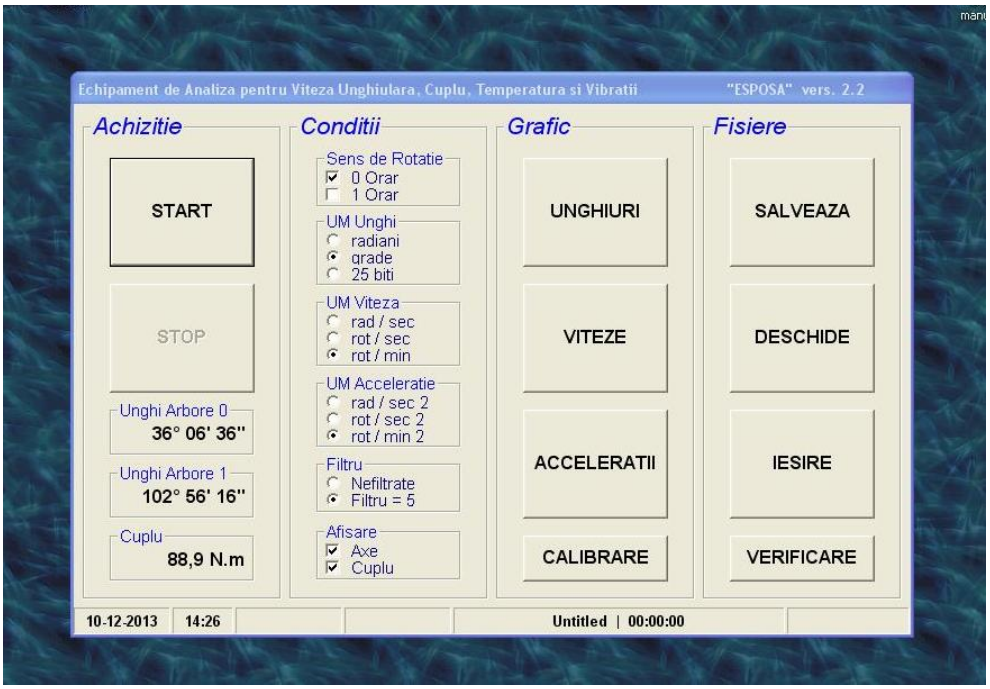

Figura 4.9. Data aquisition program screenshot

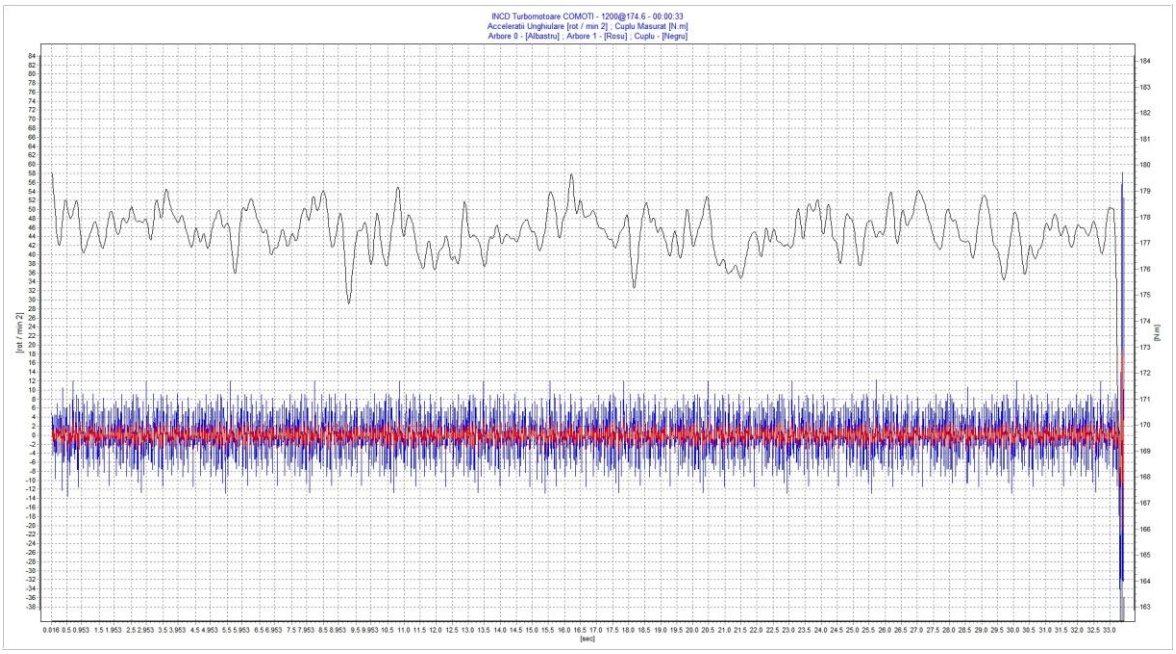

Fig. 4.10 Torque and acceleration diagram

4.1.2.3. Work procedure

Original research was carried out using a dynamic closed-circuit test rig with a turque range of 0-200 Nm, speeds in the range of 200-3000 RPM and using gears of different widths in the test box, with a view to achieve both natural number overlaps and other numbers.

Vibrograms were recorded during each test, representing the angular accereration as well as recording real-time instantaneous torque as measured by the transducer.

The last parameter was the main factor influencing the gearung operation evaluation as a function of overlap.

Two gearings of different widths were tested, the other geometrical parameters being identical. The only difference, as a consequence of the width difference, is the overlap value, equal to the unit in the standard case and equal to 0.867 in the second case. Photographs of the two gearings are shown in figures 4.11 and 4.12.

Fig. 4.11.Unit contact ratio gearing

Fig. 4.12. Lower overlap unit

The rig thus equipped is capable of measuring fundamental mechanical parameters, allowing for the evaluation of torsional vibration resulting from geometrical modifications of the studied gearing. The parameter studied with a view to compare the two gearing types is the measured torque amplitude.

4.2. Experimental results

4.2.2. Results obtained using the static meshing stiffness test rig

4.2.2.1. Experimental results

The experiments were carried out by increasing the load, starting with the lowest load and ending with the maximum, the gearing being in each case positioned in the characteristic points along the contact line, as shown in the tables below.

The laser dot reading accuracy was an important problem, the best accuracy obtained being 0.1 mm.

The contact line point was initially calibrated optically, although calipers were ultimately used due to providing a much more stable, repeatable and easily applied method.

The caliper method is also difficult to apply in this case due tu the small angular deflections, although it is easier to apply than the optical one.

Tables 4.4, 4.5 and 4.6 list the maximum dot deflections, as well as the stiffness obtained in each case.

Table 4.4 shows the result data for 50% load.

Tabel 4.4

Point on contact line	Dot deflection [mm]	Deflection angle [rad]	Meshing stiffness [Nm/rad]
A	4.7	3,48148E-04	560106
B	4.9	3,62962E-04	537245
C	4.9	3,62962E-04	537245
D	4.7	3,48148E-04	560106
E	4.9	3,62962E-04	537245

Table 4.5 shows the result data for 75% load.

Tabel 4.5

Point on contact line	Dot deflection [mm]	Deflection angle [rad]	Meshing stiffness [Nm/rad]
A	6.2	4.59259E-04	636895
B	6.3	4.66660E-04	626794
C	6.3	4.66660E-04	626794
D	6.2	4.59259E-04	636895
E	6.4	4.74074E-04	616992

Table 4.6 shows the result data for 100% load.

Tabel 4.6

Point on contact line	Dot deflection [mm]	Deflection angle [rad]	Meshing stiffness [Nm/rad]
A	8.1	6.000000E-04	650000
B	8.3	6.148148E-04	634337
C	8.3	6.148148E-04	634337
D	8.1	6.000000E-04	650000
E	8.4	6.222222E-04	626785

Table 4.7 details the point position along the contact line where tests were carried out.

Tabel 4.7

Point along contact line	Contact line coordinate [mm]
A	0
B	5,4244
C	6,5465
D	11,9689
E	17,3933

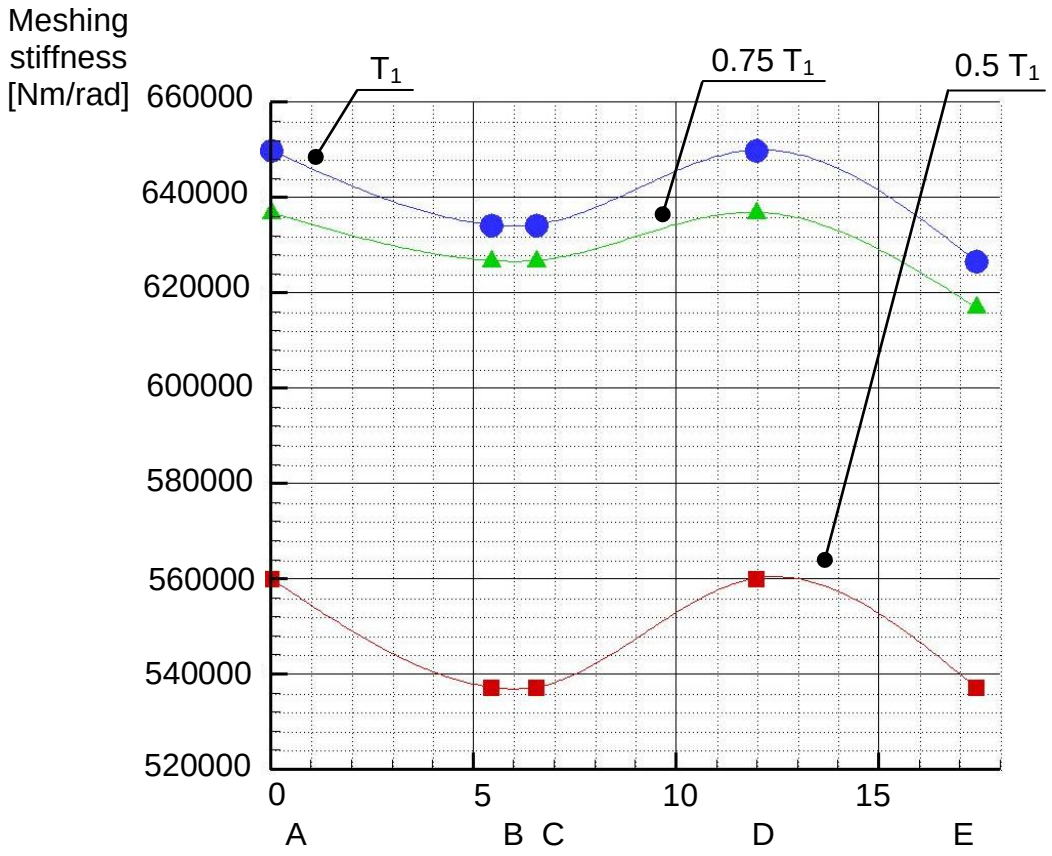

Fig. 4.13. Meshing stiffness under various loading schemes in characteristic points. (Gabroveanu, Tudor, Cănănău și Mirică, 2015).

4.2.2.2. Comparison to static theoretical results

Meshing stiffness was obtained using finite element model computation. Different numbers of elements were used along the width of the gears, resulting in different mesh densities. As expected, results varied as well.

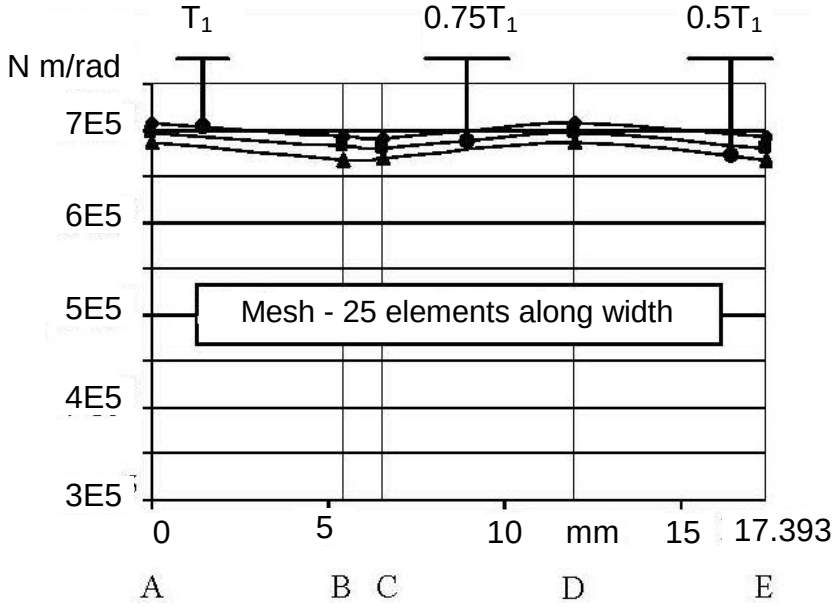

Fig. 4.14. Meshing stiffness for 25 elements along gear width (Gabroveanu, Tudor, Cănănău și Mirică, 2015)

The results obtained through the use of the finite element method are displayed in fig. 4.20 and 4.21.

The finite element model referred to here is detailed in the chapter on finite element model computation, with the number of elements along the gear width being detailed in figures 4.14 and 4.15.

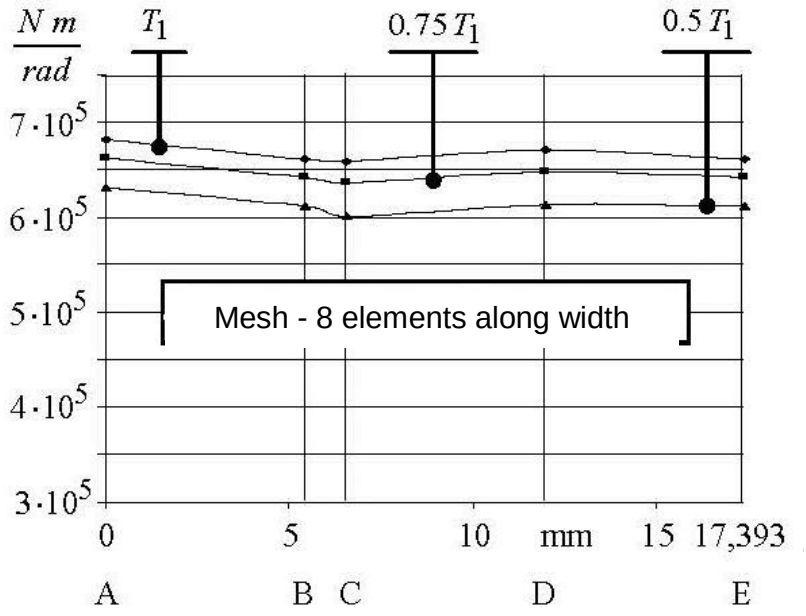

Fig. 4.15. Meshing stiffness for 8 elements along gear width (Gabroveanu, Tudor, Cănănău și Mirică, 2015)

The comparison between the computed results and the measured results was based on a maximum value, one for each applied torque series. Table 4.8 details the compared values.

Tabelul 4.8.

Table 4.8. Comparison between experimentally obtained and theoretical meshing stiffness.

Applied torque [Nm]	Maximum meshing stiffness value as measured on the test rig [Nm/rad]	Maximum computed value [Nm/rad]	
		Finite element model computation, 25 elements along width	Finite element model computation, 8 elements along width
T1	650000	710000(109.2%)	680000(104.6%)
0.75T1	636895	700000(109.9%)	670000(105.2%)
0.5T1	560106	670000(119.6%)	630000(112.5%)

A difference between the measured values and the computed values was noticed, where the measured values are smaller than the computed ones.

At smaller loads, the differences are significant,of up to 20% , while at loads close to maximum the values approach the computed ones.

In order to minimise friction,components were lubricated with a grease rich in molybdenum bisulphate. This action did not have the expected effect, as the situation did not improve noticeably.

The great differences between the reality,using a driving gear and real ball bearings with nonzero clearance fixed on flexible cases, and the finite element model, featuring points and surfaces blocked mathematically, account for the large variations in measured meshing stiffness.

4.2.2.3 Conclusions

The practical meshing stiffness evaluation method using a static test rig shows that, where a gearing with an overlap equal to a natural number is concerned, meshing stiffness in this case varies little along the contact line.

More to the point, the static test rig correctly represents the evolution of the meshing stiffness, even if there are differences between computed and measured values.

The static test rig tests confirm that the meshing stiffness variation along the contact line is smaller if the gearing overlap is a natural number.

4.2.2.4. Suggestions on the improvement of the mathod

Fundamentally, the meshing stiffness measurement method is viable, but it needs both mechanical and optical improvements in its construction.

These improvements are achievable,provided a test rig redesign is done and costs are covered.

Static test rig construction suggested improvements:

a) eliminating the ball bearings and replacing them with long ground bushing solutions (large L/D ratios);
b) increasing casing stiffness;

.

4.2.3. Dynamic test rig results

4.2.3.1 Test rig experiment preparation

At the beginning, the gearing was considered to be in the run-in period. This period ended on the dimensional stabilization of the ink spot, which occurred during tests at $0{,}5T_1$@2000 RPM, after running for 35 hours , pausing every hour.

Owing to the vibration coupling through the rigid rig structure, the vibration level due to the parametric excitation could not be evinced in the unit overlap or different and at various rotational velocities.

A vibration study was carried out, measuring instantaneous velocities and accelerations in order to highlight the vibration behaviour of the tested gearing.

4.2.3.2. Experiments

The original research was carried out using a dynamic ,closed-circuit test rig, providing the application of various torques in the range of 0-200 Nm, speeds in the range 200-3000 RPM and the use of gears of different widths in the test box with a view to achieve overlaps equal to the unit or different.

Vibrograms were recorded during each test, representing the angular accereration as well as recording real-time instantaneous torque as measured

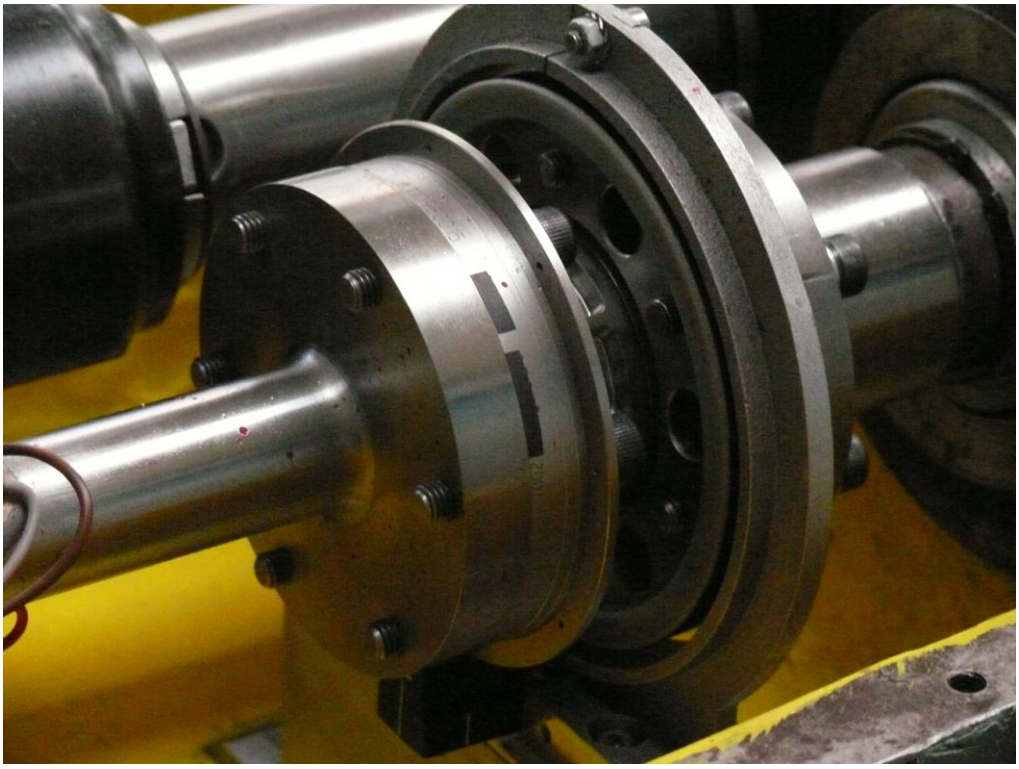

Figura 4.22. HBM T10 FS contactless torque transducer

by the transducer.

The last parameter was the main factor influencing the gearung operation evaluation as a function of overlap.

Two gearings of different widths were tested, the other geometrical parameters being identical. The only difference, as a consequence of the width difference, is the overlap value, equal to the unit in the standard case and equal to 0.867 in the second case. Photographs of the two gearings are shown in figures 4.11 and 4.12.

4.2.3.3. Experimental results

The parameter studied with a view to compare the two gearing types from the standpoint of vibration stability is:

1) Measured torque amplitude;

this parameter wasmeasured and studied for each of the cases shown below in tables 4.9 and 4.10.

4.2.3.3.1. Unit overlap experimental results

The experiments described in table 4.9 were carried out:

Table 4.9

Mt N.m	Applied rotational velocity as shown by control panel Rot/min				
	1200	1500	2000	2500	3000
0,4	X	X	X	X	X
35,9	X	X	X	X	X
79,1	X	X	X	X	X
104,8	X	X	X	X	X
174,6	X	X	X	X	X

Resulting vibrograms

The torque variation amplitude for each entry in table 4.10 was measured. The peaks were not ignored, even when due to the inexact nature of the electric operation of the AC electric motor controlled by the reconstructed wave power converter , as they were difficult to

Table 4.10

Mt N.m static	Applied rotational velocity as shown by control panel Rot/min Torque variation amplitude, Nm				
	1200	1500	2000	2500	3000
0,4	3.0	2.5	2.0	1.9	1.9
35,9	6.8	5.0	5.5	5.0	8.0
79,1	7.5	5.0	5.0	5.2	6.0
104,8	10.0	5.5	5.0	6.0	6.0
174,6	35.0	27.0	25.0	25.0	37.0

4.2.3.3.2. Reduced overlap experimental results

The experiments described in table 4.11 were carried out:.

Table 4.11

Mt N.m static	Applied rotational velocity as shown by control panel Rot/min Torque variation amplitude, Nm				
	1200	1500	2000	2500	3000
0,5	X	X	X	X	X
35,7	X	X	X	X	X
87,6	X	X	X	X	X
104,8	X	X	X	X	X

Resulting vibrograms

Table 4.12 contains the torque amplitudes measured in the same conditions as the preceding case involving unit overlap. The measurements carried out are described in table 4.11.

Table 4.12

Mt N.m static	Applied rotational velocity as shown by control panel Rot/min Torque variation amplitude, Nm				
	1200	1500	2000	2500	3000
0,5	6.2	6.2	7.0	7.7	9.0
35,7	7.0	8.0	6.6	6.5	7.6
87,6	7.5	7.5	6.0	5.8	7.0
104,8	9	7	6	5.8	8.0

The torque variation amplitudes will henceforth be compared, assuming constant speed and applied torque from a static standpoint, with a view to evince the behaviour of the two gearing types, one featuring unit overlap and the other a reduced overlap.

4.2.3.3.3. Experimental result comparison for the two gearing types

In order to evaluate the results, the graphical plot of torque amplitude as a measure of meshing parametric excitation was selected as the most evocative representation.
Figure 4.23 showcases the torque amplitude variation under reduced torque loading for both gearings.

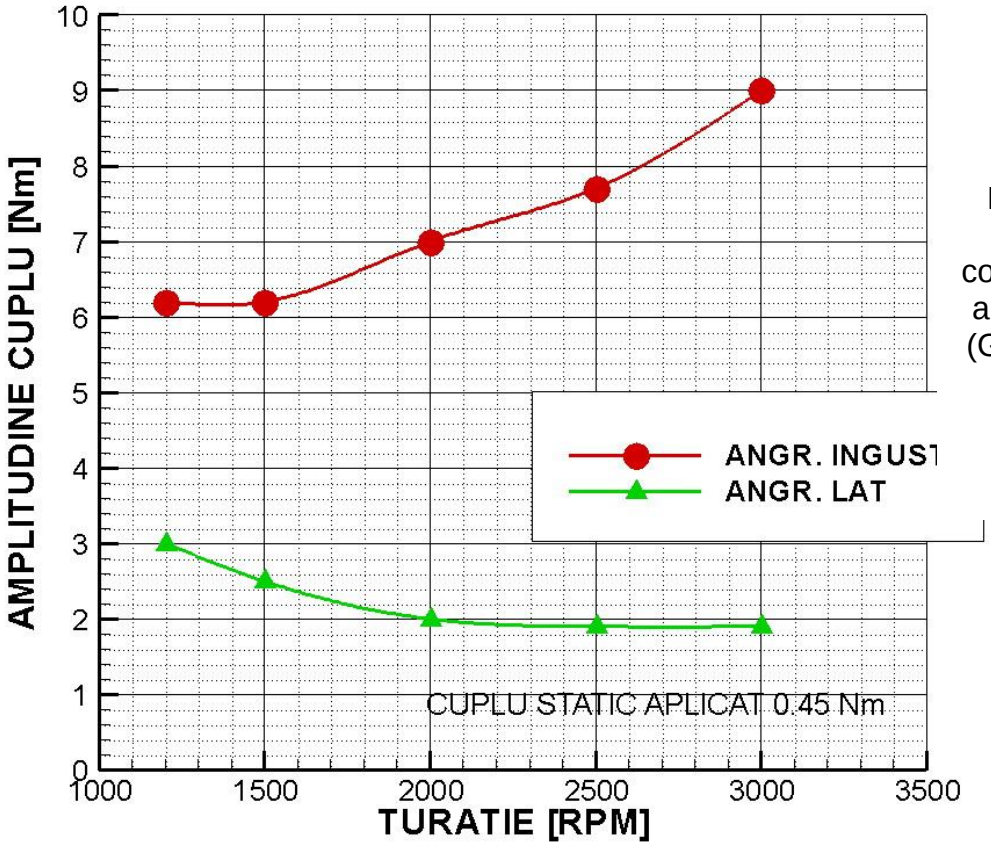

Fig. 4.24. The two gearing types compared at 0.45 Nm applied static torque (Gabroveanu, Tudor, Cănănău, Mirică, 2015).

A tendency towards stabilization is observed in the unit overlap gearing as speed increases, while the opposite tendency is observed in the reduced overlap gearing.

Figure 4.24 displays the torque amplitude variation for increased applied static torque.

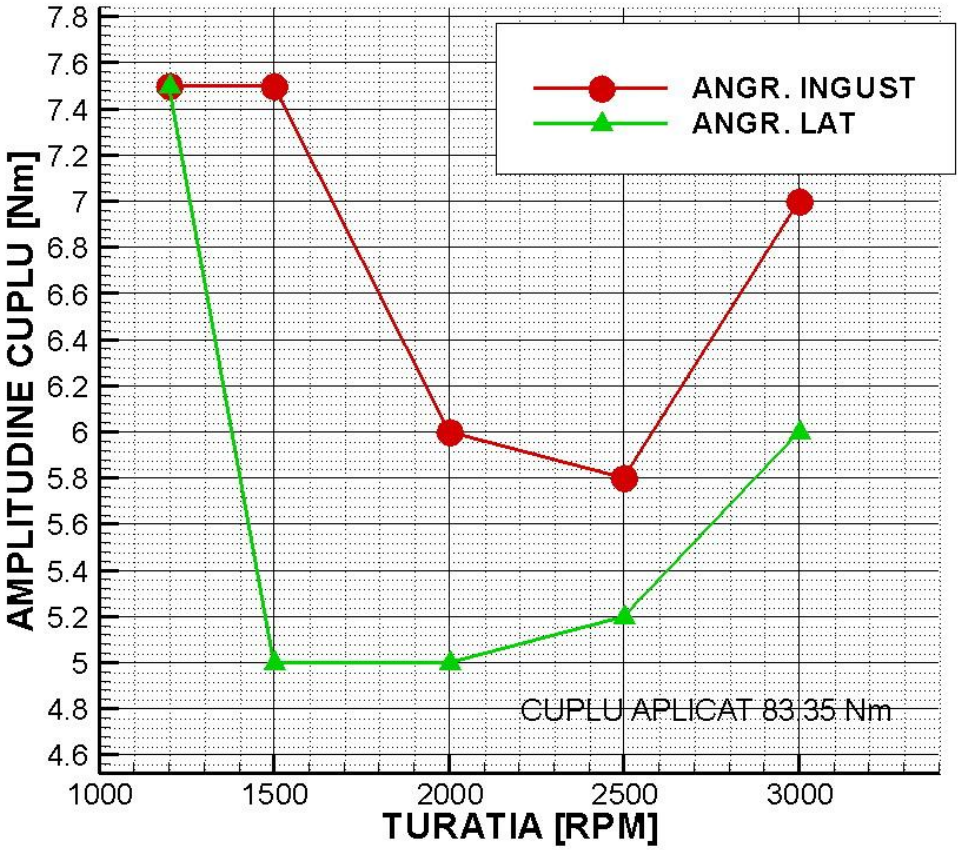

Fig. 4.24. The two gearing types compared at 83.35 Nm applied static torque (Gabroveanu, Tudor, Cănănău, Mirică, 2015).

This is repeated when applied torque is increased, specifically the unit overlap is more stable than the reduced case.

The reduced overlap gearing displays increased instability when compared to the unit overlap gearing.

Figure 4.26 displays the same comparison at a static load of 104.8 Nm.

Tests at the nominal static torque of 174.6 Nm could not be carried out on the reduced overlap gearing. This was due to an extremely high degree of instability of the torque amplitude as measured by the transducer, as the applied torque values could not be maintained due to the tapered assembly repeatedly unloading during tests.

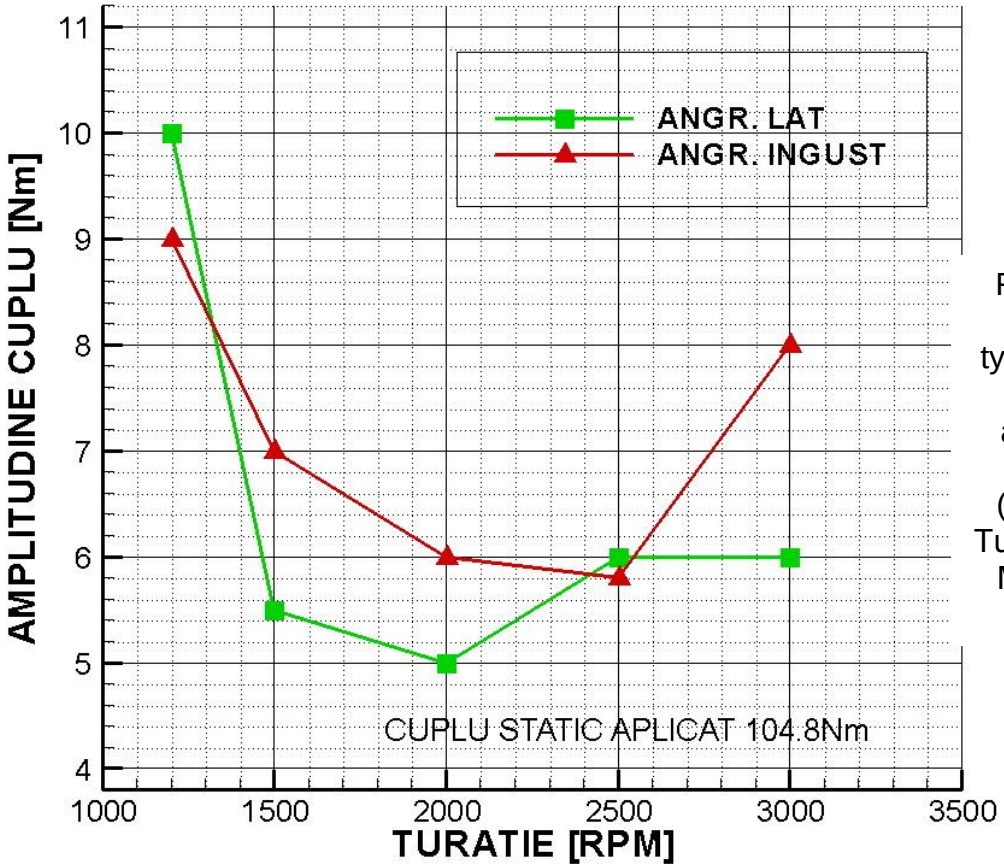

Fig. 4.24. The two gearing types compared at 104.8 Nm applied static torque (Gabroveanu, Tudor, Cănănău, Mirică, 2015). Nm.

All cases shown in the tables above allow for similar comparisons between normal width and modified width gearings.

All cases studied display similar, incomparably better behaviour where the unit overlap gearing is concerned, as opposed to the lower overlap gearing.

In my opinion, this experimentally observed fact confirms both the finite element method-obtained results, as well as the results obtained using MSC ADAMS, confirming the fact that the meshing stiffness variation is much lower in gearings with natural number overlap that in whole number overlap.

4.3. Conclusion

The developed test rig allows for the study of meshing stiffness, depending on the gearing geometry, by studying its effects on the torque amplitude variations in the assembly.

The torque variation amplitude as a factor describing the gearing stability from the standpoint of parametric excitation is the novel element the dynamic test rig introduces. Through its design, this modified, improved test rig clearly evidences the influence of the overlap over the gearing vibration stability.

Concerning the dynamic test rig, it is worth mentioning that it a state of the art installation on par with similar installations in other research institutions in countries with vast experience in this subject .

Similar comparisons between the normal width and modified width gearings can be made for all cases shown in the tables for which tests were carried out.

5. FINAL CONCLUSIONS

5.1. Summary of research carried out

The present paper deals with considerations on computation through modern means of heavily loaded parts, as well as experimental problems, with a very broad spectrum of activity.

The subjects below were expanded upon.

1. The state of the art of theoretical and experimental research was studied .

This study revealed the following:

1. The reduction of parametric excitations in gears shows great promise, especially where wide gearbox transmissions are being used, where profile corrections are very difficult or even impossible to achieve.
2. The finite element method must be compared to an experimental study.
3. The finite element method is widely used and well equipped to solve highly complex engineering problems.
4. Seeing as dynamically simulating gearing operation is possible, this is an option that needs to be explored.

The study of the state of the art also revealed the following aspects:

1. The test rigs used are mainly closed-circuit for well-known reasons (the ability to apply large loads, efficiency).
2. the equipment used to evince vibration levels are not only piezoelectric (vibration transducers) but also optical precision encoders, as was suggested by the author of this paper .
3. The test rig requires high technology equipment in order to ensure repeatability as well as the ability to calibrate the equipment..

2. Theoretical research was carried out and theoretical contributions were made, the most important of which are:

1. The application of the finite element method to meshing stiffness studies;
2. The application of simulation techniques to dynamic gearing simulation ;
3. The application of mechanism dynamics software to vibration level study in dynamic gear test rigs;

4. The design of solutions for equipping a gear test rig with measurement and real time, high sample frequency data aquisition equipment.

3. The research and experimental contribution constitute another complex problem. They are summarized below

…

5.2. Own contribution

5.2.2. Theoretical contributions

To summarize, this paper makes the following theoretical contributions:

1. The development of a method for using the finite element method to study meshing stiffness;
2. The development of a method for the use of mechanism dynamic operation software;
3. The theoretical and experimental validation of the idea that gearing with natural number overlap encounter far lower parametric excitation, being naturally suited for the use in turbomachinery transmission where toothing corrections cannot be applied due to the large gear width .

5.2.3. Experimental contributions

The important experimental contributions are:

1. Support for using precision optical encoders to measure internal excitation and resonance in gearings.
2. The design and development of a static meshing stiffness test rig which features numerous advantages, of which noteworthy are the simplicity, the rapid conversion and the low cost involved.